Characterizing the role of mitochondrial dysfunction in Autosomal Recessive Spastic Ataxia of Charlevoix-Saguenay (ARSACS)

By

Patrick Adam Bouchard

Integrated Program in Neuroscience
McGill University

Montreal, QC

August 2015

A thesis submitted to McGill University in partial fulfillment of the degree of Master of Science

Abstract

Autosomal Recessive Cerebellar Ataxia of Charlevoix-Saguenay (ARSACS) is a complex inherited neurodegenerative disorder. First described in Quebec in 1978, ARSACS is caused by mutations in the *SACS* gene that encodes the giant protein of 4579 amino acids, Sacsin. Sacsin has been localized to mitochondria and the cytoplasm, but its function is unknown, and as a result the pathological mechanisms of this complex disease are currently poorly understood. Two features of ARSACS are intermediate filament bundles and elongated mitochondria. The purpose of this project was to evaluate mitochondrial function and to test the hypothesis that mitochondrial abnormalities in ARSACS are a downstream consequence of disordered intermediate filaments. To this end, two cellular models were used: motor neurons in *Sacs*$^{-/-}$ mouse-derived spinal cord-dorsal root ganglion (DRG) cultures and cultured skin fibroblasts derived from patients. Neurofilament bundling and a modest, but statistically significant, increase in length of mitochondria in motor neuron dendrites were observed after three weeks *in vitro*. This increase in mitochondrial length was more evident in fibroblasts cultured from ARSACS patients. Human fibroblasts also demonstrated similar bundling of vimentin intermediate filaments, validating the relevance of this model to the neuronal phenotype. With regard to interrogation of mitochondrial function, BN-PAGE of fibroblast mitochondria determined no difference in respiratory chain complex abundance or assembly, and bromouridine incorporation demonstrated no significant change in localization of newly synthesized mitochondrial RNA to RNA granules. Additionally, this study evaluated an intermediate filament-related phenotype that encompasses proteins involved in anchoring of the cytoskeleton to the nucleus (nesprin), consistent with displacement of organelles caused by bundling of intermediate filaments.

Finally, to further examine the relationship between intermediate filament and mitochondrial phenotypes in ARSACS, these parameters were measured in fibroblasts from patients with Giant Axonal Neuropathy, a generalized disorder of intermediate filament organization. While intermediate filament bundling and displacement of nesprin and endoplasmic reticulum were found in both ARSACS and GAN fibroblasts, the latter cell line exhibited no change in mitochondrial length. This study provides evidence that changes in mitochondrial morphology observed in ARSACS are not a direct secondary effect that arises from the collapse of the intermediate filament network.

Résumé

L'ataxie spastique autosomale récessive de Charlevoix-Saguenay (ARSACS) est une maladie neurodégénérative héréditaire. Décrite au Québec en 1978, l'ARSACS est causée par des mutations du gène SACS, codant pour la sacsine. La sacsine est une protéine de 4579 acides aminés, présente dans le cytoplasme et à la surface des mitochondries. Sa fonction reste inconnue et les mécanismes physiopathologiques responsables de la maladie sont peu compris. Les deux caractéristiques principales observées dans l'ARSACS sont l'agrégation des filaments intermédiaires et l'élongation des mitochondries. Cette étude consiste donc à évaluer la fonction mitochondriale dans l'ARSACS et à vérifier l'hypothèse selon laquelle les anomalies mitochondriales seraient la conséquence de la perturbation du réseau des filaments intermédiaires. Deux modèles cellulaires ont été utilisés : 1) des cultures primaires de neurones moteurs issus des ganglions de la racine dorsale de la moelle épinière des souris *Sacs -/-*, 2) des fibroblastes dérivés de patients ARSACS.

Dans les neurones moteurs à trois semaines de culture, nous avons observé une augmentation modeste mais significative de la longueur des mitochondries au niveau des dendrites, ainsi que la formation d'amas de neurofilaments. L'hyperfusion des mitochondries était plus évidente dans les fibroblastes dérivés de patients. Nous y avons de plus observé l'agrégation des filaments de vimentine, validant ainsi leur utilisation comme modèle de l'ARSACS. L'étude des complexes de la chaine respiratoire par électrophorèse en gel natif (BN-PAGE) n'a montré aucun déficit de leur assemblage. L'étude des ARNm mitochondriaux nouvellement synthétisés après incorporation de bromodeoxyuridine montre une localisation normale au sein des granules d'ARN. Ensuite, cette étude a évalué un phénotype associé au

déplacement des organites par l'amas de filaments intermédiaires, surtout au niveau des protéines impliquées dans l'ancrage du cytosquelette au noyau cellulaire (nesprine3).

Finalement, afin de mieux comprendre la relation entre l'altération des filaments intermédiaires et celle des mitochondries dans l'ARSACS, les mêmes paramètres ont été étudiés dans les fibroblastes de patients atteints de neuropathie à axones géants (GAN), une maladie de l'organisation des filaments intermédiaires. Nous avons mis en évidence une agrégation des filaments intermédiaires, couplée à une altération de la morphologie du réticulum endoplasmique et de la localisation de la nesprine dans l'ARSACS et la GAN. En revanche, aucun changement de la morphologie mitochondriale n'a été observé dans les fibroblastes GAN. Ceci démontre que l'hyperfusion mitochondriale observée dans les fibroblastes de patients ARSACS n'est pas une conséquence directe de la perturbation du réseau de filaments intermédiaires.

Acknowledgements

I'd first like to thank my supervisors, Dr. Heather Durham and Dr. Eric Shoubridge for taking in a very lost student and providing him with direction, encouragement and mentorship. Your boundless passion for your work is something that I hope to emulate in my future endeavors. To the members of the Durham and Shoubridge labs, I'd like to thank you all for making my time here fulfilling, rewarding and fun.

To Dr. Benoit Gentil, for providing your knowledge and guidance in preparing experiments and for your blunt honesty when I needed the push. To Dr. Hana Antonicka for your help and patience in troubleshooting a number of my experiments. To Sandra Minotti, for preparation and maintenance of cultures vital to my project as well as great company in the lab. To Michael Tibshirani for your friendship, understanding far too many of the references I make and always providing some form of musical stimulus. To Kyle St. Louis (past member), for being an excellent desk-mate and friend. To Dr. Woranontee Weraarpachai for her great help in running through my BN-PAGE experiments. Thank you to my mentor, Dr. Jean-François Cloutier and to members of my supervisory committee, Dr. Heidi McBride and Dr. Jason Young.

To Liane Levasseur and Joe Pogson, I thank you both incredibly for the friendship, support and adventures you've shared with me over my time here.To Alex Janer, Vincent Paupe, Shamisa Honarmand, Kathleen Daigneault, Isabella Straub, Olga Zurita Rendon, Ayumu Seguira, Karine Doiron, Sevan Mattie, Julien Prudent, Roxanne Larivière and Nicolas Sgarioto, the sheer magnitude of this list highlights how lucky I was to have been able to do my research with such an incredible group of kind, caring people. To everyone in the basement of the Neuro, it was a pleasure getting to know you / play hockey/basketball/softball/dodgeball with you all. I'll miss you all very much!

I also would like to acknowledge my family and friends in Ottawa for their support in putting out a perfectly cromulent thesis. I want to thank my parents, Denis and Linda, for the innumerable amounts of visits, drives home and ineffable encouragement in more ways than I can possibly mention through both this degree and my life. A thank you to my big brother Marc for setting an example I will always strive to follow. Finally I'd like to thank my partner in crime, Diane Nakamura. Over the last three years, through all the stress and panic, you've been there to keep me centered, sane and happy. Completing this thesis has only been possible with you at my side. You're my rock.

List of Figures

Introduction

Inherited ataxias are rare disorders with diverse causes and a dearth of effective therapeutics. ARSACS is one such disease, caused by mutation in the *SACS* gene and loss of function of the protein sacsin (Engert et al., 2000). Typically, ARSACS presents in early childhood with progressive cerebellar ataxia, spastic paraplegia and motor-sensory neuropathy, which leads to a significant decrease in mobility and death in the fifth decade (Bouchard, Barbeau, Bouchard, & Bouchard, 1978). Current treatments are mainly symptomatic and the overall mechanism by which mutations cause disease remains unknown.

The sheer size and complexity of the sacsin protein is a likely element in the multifactorial nature of ARSACS. Sacsin has been shown to localize to both the cytoplasm and mitochondria, and a number of domains have been implicated in DNA repair, protein unfolding, and the ubiquitin-proteasome system, hinting at a multifaceted role in proteostasis and chaperone activity (Kozlov et al., 2011). However, the massive nature of the protein has stymied thorough assessment of its biological function. One theory is that sacsin loss of function provokes a dysregulation of mitochondrial homeostasis and possibly chaperone activity, which in turn causes a number of downstream effects. Since abnormal bundling of neurofilaments is a prominent finding, another theory is that ARSACS is primarily a disorder in neurofilament organization (Girard et al., 2012; Lariviere et al., 2014). This study used both mouse and human models of ARSACS to examine parameters of mitochondrial function and the role played by disorganization of the intermediate filament network.

Chapter 1: Literature review

What is ARSACS?

Autosomal Recessive Spastic Ataxia of Charlevoix-Saguenay (ARSACS) is a complex, inherited, and progressive neurological disorder with symptoms characterized by a triad of cerebellar ataxia, pyramidal tract defects and peripheral motor-sensory neuropathy (Bouhlal, Amouri, El Euch-Fayeche, & Hentati, 2011; Pedroso et al., 2011). Originally studied in the regions surrounding Charlevoix and Saguenay-Lac Saint Jean in northeastern Quebec, the disorder was first described in 1978 by Bouchard et al. (Bouchard et al., 1978; De Braekeleer et al., 1993; Takiyama, 2006). The inhabitants in that region have a carrier prevalence of about 1/22 due to the founder effect of Quebec colonization in the 17th century (De Braekeleer et al., 1993). In the year 2000, the *SACS* gene was identified by Engert *et al.* as the gene responsible for ARSACS (Engert et al., 2000). Since the identification of the gene in patients from Quebec, it has been described worldwide, with cases identified in Brazil, Tunisia, France and Japan, among others (Anheim, 2011; Gomez, 2004; Miyatake et al., 2012; Mrissa et al., 2000; Ogawa et al., 2004; Pedroso et al., 2011; Thiffault et al., 2013). However, the initial population in Quebec remains the most studied.

Clinical aspects and diagnosis

As is common in autosomal recessive cerebellar ataxias, ARSACS is marked with early-onset of spasticity of the lower limbs, generally presenting in the form of unsteady gait in infants at ages of 12 to 24 months (Bouhlal et al., 2011; Fogel & Perlman, 2007). In the visual system, nystagmus and saccadic movement defects in smooth pursuit are among other early symptoms, as is hypertrophy of the retinal nerve and radiation of myelinated fibers from the optic disk (Garcia-Martin et al., 2013; Pablo et al., 2011; Yu-Wai-Man et al., 2014). Speech defects such as

explosive speech, slurring and dysarthria appear and persist through development (Bouchard et al., 1978; Ogawa et al., 2004). Physiologically, distal muscle wasting, bone deformation of the feet and altered tendon reflexes comprise the musculoskeletal symptoms of ARSACS (Bouchard et al., 1978).

In adolescence, pyramidal tract defects, ataxia and neuropathic symptoms progress. In early adulthood, there is an increase in deep tendon reflexes and muscle tone uncharacteristic of other inherited spastic ataxias (Anheim, 2011). In the late twenties, most tendon reflexes are blunted and electromyography demonstrates reduced nerve conduction velocities and denervation of distal muscles, indicating progressive distal neuropathy. Nerve biopsies conducted on patients confirm peripheral myelinopathy and severe axonal degeneration while muscle biopsies revealed neurogenic atrophy (Bouchard et al., 1998; Grieco et al., 2004; Terracciano et al., 2009). Disability generally requires the use of a wheelchair at roughly age 40, and death follows at a mean age of 51 years (Bouhlal et al., 2011; Takiyama, 2006). On autopsy, Purkinje cell loss and storage of neuronal lipids was noted (Girard et al., 2012). While many of these symptoms are similar throughout all ARSACS cases, there have been unusual cases of ARSACS, with some lacking spasticity (Shimazaki, Sakoe, Niijima, Nakano, & Takiyama, 2007) or retinal hypermyelination (Ouyang et al., 2008), and some others exhibiting mild mental retardation (Kamada, Okawa, Imota, Sugawara, & Toyoshima, 2008). It is possible that the differences are mutation-specific or vary based on genetic background (Miyatake et al., 2012).

With regards to diagnosis, genetic testing can be performed when ARSACS is suspected; however, quantifiable coordination tests such as the Nine Hole Peg Test (NHPT) and finger-nose

tests are currently used to assess ARSACS. Unfortunately, the slow clinical progression of the disease and the vague indicators of coordination based on two reaction-time based tests is relatively inefficient at diagnosing ARSACS. However, a recent study using the Virtual Peg Insertion Test (VPIT), a haptic feedback virtual reality assessment, has shown promise in evaluating coordination more thoroughly in ARSACS patients (Gagnon et al., 2014).

Sacsin structure and function

The *SACS* gene was identified in 2000 through positional cloning as the gene responsible for ARSACS (Engert et al., 2000). Located on chromosome 13 (13q11), linkage disequilibrium analysis initially showed that *SACS* was a single exon of a length of 11 487 bp, placing it among the largest encoded genes in vertebrates (Engert et al., 2000). However, the development of more rigorous molecular techniques and analysis of ARSACS patients lacking any mutations in the giant exon, uncovered many small exons upstream of the *SACS* giant exon, with a total of 11 exons being described within the gene (Vermeer et al., 2008). The largest transcript encodes a protein with a length of 4579 amino acids with a molecular weight of 520 kDa. In ARSACS cases from the Charlevoix-Saguenay region, the 6594delT mutation is the most common, with a smaller population having a 5254C->T nonsense mutation (Engert et al., 2000; Thiffault et al., 2013). The common feature of these and other mutations that cause ARSACS is the truncation or downregulation of sacsin protein, implying a loss of function mutation responsible for ARSACS pathology (Thiffault et al., 2013). Regrettably, the enormous size of both the gene and the protein have hindered biochemical studies of sacsin function in both cellular and animal models.

The overall function of sacsin is unknown; however, some functional attributes of certain protein domains can be inferred through comparison of domain homology. Sacsin is highly

conserved in vertebrates, with at least 93% amino acid sequence identity in mammals, 83% in reptiles and 68% in fish (Romano et al., 2013). Sacsin comprises 7 distinct protein domains identified by sequence homology. From amino-terminal to carboxy-terminal, sacsin has a **ubiquitin-like domain (UbL),** three **sacsin repeating regions (SRRs),** a putative XPC binding **(XPCB)** domain**,** a **DnaJ** domain and a higher eukaryote and prokaryote nucleotide-binding (**HEPN**) domain (J. F. Anderson, Siller, & Barral, 2010, 2011; Grynberg, Erlandsen, & Godzik, 2003; Kamionka & Feigon, 2004; Parfitt et al., 2009) (Figure 1) (Romano et al., 2013)**.**

Functional breakdown of sacsin

The UbL domain at sacsin's N-terminus interacts with the proteasome, as shown in co-immunoprecipitation experiments performed by Parfitt *et al.* in 2009, indicating a potential functional link to the protein degradation machinery (Parfitt et al., 2009). The three SRRs were described in 2010 by Anderson *et al.* as having a trio of large repeated domains (roughly 360 residues) with Hsp90-like ATPase activity at their N-terminali, with the second domain being significantly shorter than the others (J. F. Anderson et al., 2010). Interestingly, this activity could be abolished by introduction of an ARSACS-associated mutation at the 2nd SRR N-terminal, indicating a possible functional role of Hsp90-like chaperone activity in sacsin, as well as demonstrating that the presence of a trio of SRRs does not imply redundant function in the repeated region (J. F. Anderson et al., 2010). Later functional mapping further elaborated the SRR domains into repeating subregions as shown in Figure 1 (Romano et al., 2013). The XPCB domain following the SRRs has significant sequence identity with human HR23A, a protein involved in both nucleotide excision repair and the ubiquitin-proteasome system (UPS), though a binding partner of the sacsin XPCB domain has yet to be identified (Kamionka & Feigon, 2004).

DnaJ represents the key functional domain of DnaJ/Hsp40 class co-chaperones, which are implicated in protein folding through their enhancement of Hsp70 ATPase and substrate binding activity. In sacsin, this domain is active and has shown protective effects in mediating aggregation caused by other ataxia-causing proteins such as ataxin-1 (Parfitt et al., 2009). This provides a functional link between ataxia and defective chaperone activity. A compound heterozygous mutation that causes ARSACS (K1715X/R4331Q) targets regions on both the DnaJ and SRR domains; however, the individual mutations yield no phenotype. This also indicates that the sacsin DnaJ domain may interact with the SRR regions upstream (Vermeer et al., 2008). Finally, at the carboxy-terminus of the sacsin protein is the HEPN domain**.** This domain binds nucleotides and dimerizes with other HEPN containing proteins (Grynberg et al., 2003). Kozlov *et al.* noted that while HEPN bound nucleotides such as ATP and GTP, it had no ATPase or GTPase activity of its own. Nucleotide binding may thus act as a mechanism for energy storage for sacsin's upstream chaperone activity (Grynberg et al., 2003; Kozlov et al., 2011). A common factor in sacsin mutations leading to the most severe ARSACS phenotypes is the loss of function or large-scale deletion of C-terminal protein domains, specifically HEPN and DNAJ. Many proteins in inherited ataxias, such as spinocerebellar ataxia and Friedrich's ataxia, share common interacting partners, hinting at a functional link between their molecular pathologies. Like many neurodegenerative disorders, ataxias are characterized by disturbed protein homeostasis that will provoke increased activity from both molecular chaperones and the UPS. The individual domains of sacsin protein have been shown to interact with both the UPS and molecular chaperones known to target misfolded proteins. Sacsin is expressed in the brain, with high levels of expression in Purkinje cells, paracerebellar nuclei and both corticospinal and cranial motor neurons.

ARSACS in human patients and knockout models

Decrease in the number of Purkinje cells was noted in both ARSACS brains obtained at autopsy and in Sacs$^{-/-}$ mouse brains (Girard et al., 2012). In cultured fibroblasts derived from ARSACS patients, cultured primary mouse hippocampal neurons and cultured SH-SY5Y cells, sacsin partially co-localized to mitochondria by immunocytochemistry, indicating a possible role of sacsin in mitochondrial dynamics (Parfitt et al., 2009). Moreover, in 2012, Girard *et al*. assessed mitochondrial structure and function in a number of ARSAC models (Girard et al., 2012). In both cultured ARSACS patient fibroblasts and Sacs$^{-/-}$ mouse primary hippocampal neuron cultures, the presence of bulbous, hyperfused mitochondrial networks could be indicative of defects in mitochondrial fission/fusion machinery or other underlying mitochondrial dysfunction. This is supported by the discovery of interaction between sacsin and dynamin-related protein-1 (Drp1), a regulator of mitochondrial fission (Girard et al., 2012). Additionally, sacsin knockdown in SH-SY5Y cells by siRNA resulted in a significant decrease in mitochondrial membrane potential, indicative of impaired oxidative phosphorylation (Girard et al., 2012). Finally, in *Sacs*$^{-/-}$ mouse brain slices, proximal dendrites were thicker and more disorganized than their wild-type counterparts (Girard et al., 2012). Other models of mitochondrial dysfunction (such as Drp1 KO in *Drosophila* and an Alzheimer's mouse model generated with a mitochondrial inhibitor) show a characteristic pattern of dendritic thickening, possibly due to the role of mitochondria as local ATP sources and regulators of calcium concentration within the cell (Szabados et al., 2004; Verstreken et al., 2005). However, a characteristic finding is the accumulation of neurofilaments in the somatodendritic region, which would also alter dendritic morphology (see below) (Lariviere et al., 2014).

Mitochondrial structure and function

Mitochondria are eukaryotic organelles critical for regulation of cellular function including energy metabolism, cell signaling and calcium buffering (Duchen & Szabadkai, 2010). Mitochondria are highly dynamic as well, forming an interconnected network that is regulated by both fission and fusion events. Fission is thought to allow for the isolation of dysfunctional mitochondrial compartments for mitophagy, while fusion is thought to have a protective role in equilibrating the contents of the matrix to protect against DNA damage caused by oxidative stress (Chen & Chan, 2009). Fusion and fission reactions are mediated through mitofusin 1 and 2, and Drp1, respectively, the latter of which has been shown to interact with the sacsin N-terminal region (Girard et al., 2012; Legros, Lombes, Frachon, & Rojo, 2002; Song, Ghochani, McCaffery, Frey, & Chan, 2009). When homeostasis of these fusion and fission processes is disrupted, this network becomes either elongated or fragmented and efficient mitophagy can be hampered, leading to an overabundance of malfunctioning mitochondria. Endoplasmic reticulum interacts with mitochondria through mitochondria-associated membranes (MAMs), a contact structure that forms an interface between both organelles, linking the membranes without homogenizing them. These contacts have a critical regulatory role in mitochondrial dynamics, calcium transfer, biogenesis of mitochondria and exchange of lipids (de Brito & Scorrano, 2010; Rizzuto et al., 2009).

The mitochondrial genome is much smaller than that of the eukaryotic nucleus, encoding 22 transfer RNAs and two ribosomal RNAs as well as 13 core proteins involved in the oxidative phosphorylation (OXPHOS) pathway(S. Anderson et al., 1981). Mutations to this compact

genome lead to severe neuromuscular diseases and myopathies, generally through disruption of Adenosine triphosphate (ATP) synthesis(Martikainen & Chinnery, 2015).

The compartmentalization of the mitochondrial matrix at the level of transcription and replication is less well-characterized than that of the nucleus or cytosol. Mitochondrial DNA is localized within the organelle in protein-DNA complexes called nucleoids, which are between 50 and 300 nm in diameter (Busch, Kowald, & Spelbrink, 2014a). These complexes are exchanged during fission events and are key spatial regulators of replication and downstream OXPHOS complex assembly (Kowald & Kirkwood, 2011). At the mtDNA level, mutations accumulate unevenly over time due to repair errors and oxidative phosphorylation byproducts. Damaged mtDNA can expand to other mitochondria through fission and fusion events and lead to heteroplasmy, wherein a single cell will contain both wild-type and mutant mtDNA (Busch, Kowald, & Spelbrink, 2014b). The understanding of how replication and quality control of the nucleoid is regulated is a key factor in comprehending the development of mitochondrial diseases (Detmer & Chan, 2007).

At the level of mtRNA transcription, newly transcribed RNA is localized in discrete foci known as RNA granules (Antonicka, Sasarman, Nishimura, Paupe, & Shoubridge, 2013). A posttranscriptional processing enzyme, RNase P, colocalizes with these granules, as do several RNA-binding proteins such GRSF1 and FASTKD2. The former binds 3 specific G-rich RNA species and is required for processing of new mtRNA transcripts while the latter is a marker of mitochondrial RNA granules(Antonicka et al., 2013). Inhibition of transcription by actinomycin D or ethidium bromide (EtBr) treatments has been shown to disrupt RNA granule formation (Antonicka et al., 2013).

Mitochondria produce energy through oxidative phosphorylation, a mechanism whereby electron transfer takes place within mitochondrial cristae to generate a proton electrochemical gradient across the inner mitochondrial membrane. This gradient drives the synthesis of ATP, the energy currency of the cell. The proton gradient is generated through a series of redox reactions across OXPHOS complexes I through IV, with ATP synthase (Complex V) using the protons to drive the phosphorylation of adenosine diphosphate (ADP) (Chaban, Boekema, & Dudkina, 2014). Complex I, NADH dehydrogenase, is the first entry point of the electron transport chain (ETC) and is responsible for binding NADH and stripping two of its electrons and transferring them to ubiquinone (Coenzyme Q). The conformational change induced by ubiquinone reduction allows complex I to translocate 4 protons across the membrane, initiating the proton gradient. Complex II is an independent entry point to the ETC and oxidizes succinate and transfers electrons to Coenzyme Q. Complex III is ubiquinone cytochrome *c* reductase and oxidizes ubiquinol to ubiquinone. This allows it to pump two protons to the intermembrane space while passing electrons from ubiquinol to cytochrome *c*. Complex IV, cytochrome *c* oxidase, oxidases reduced cytochrome *c* and the electrons from this reaction are transferred to an oxygen molecule to generate water. In the process, four protons are pumped to the intermembrane space. Finally, complex V (ATP synthase), 15-18 subunit complex with a mass of roughly 600 kDa, converts energy stored in the proton gradient to phosphorylate ADP into ATP. The F_0 complex acts as an ion channel and funnels protons through to the mitochondrial matrix to generate energy sufficient to drive the F_1 complex to synthesize ATP. As protons pass through the proton channel, the central stalk and c ring will rotate. This change in binding conformation catalyzes the synthesis of ATP.

Mitochondria and neurological disease

Dysfunction at the level of fission and fusion can be an indicator of neurodegenerative disease, having been linked to Charcot-Marie-Tooth (CMT), Alzheimer's, Parkinson's and Amyotrophic Lateral Sclerosis (ALS) (Friedland-Leuner, Stockburger, Denzer, Eckert, & Muller, 2014; Gentil et al., 2012; Reddy et al., 2011; Tan, Pasinelli, & Trotti, 2014; Wang et al., 2013). In Alzheimer's disease, tau and amyloid pathology has been linked to an increase in reactive oxygen species (ROS) and a decrease in mitochondrial length concomitant with a decrease in fusion proteins OPA1, Mfn1 and Mfn2 (Hroudova & Singh, 2014). In a model of CMT, mitochondrial length and rate of fusion were decreased and directional axonal transport was impaired, although mitochondria exhibited an aberrant 'wiggling' movement (Gentil et al., 2012; Tradewell, Durham, Mushynski, & Gentil, 2009). In models of ALS due to missense mutations in *SOD1*, an increase in mutant SOD1 recruitment to mitochondria was linked to an increase in ROS generation through dysregulation of dismutase activity within the mitochondrial intermembrane space (Vehvilainen, Koistinaho, & Gundars, 2014). Parkinson's disease models demonstrated defects in oxidative respiration and more strikingly, mitochondrial quality control through PINK1 and parkin. Defects in either of these proteins were correlated to drastic increases in mitophagy and localization changes in cell models (Grenier, McLelland, & Fon, 2013) [53]. However, those disorders were associated with smaller, fragmented mitochondria rather than the longer mitochondria found in ARSACs.

Neuronal cytoskeletal architecture: Neurofilaments

The neuronal cytoskeleton is composed of microfilaments, microtubules and neurofilaments. The microtubule is a structural element composed of tubulin and is responsible

for bidirectional transport across long distances within the cell (Conde & Caceres, 2009). Moreover, in mature neurons, a large proportion of microtubules are extremely stable, with half-lives many times longer than in immature neurons (hours compared to minutes) (Baas & Black, 1990). Microfilaments are formed of actin and have a number of roles in the cell. Some cellular actin forms short (1.5-2 μm) branches perpendicular to the plasma membrane, while other actin populations align with dendrites and axons in neurons and assist in local movement of cellular cargo (Bearer & Reese, 1999; Fifkova & Delay, 1982).

Neurofilaments (NFs) are the intermediate filaments of neurons and provide both mechanoresistance and stability to cells as well as participate in signaling. NFs in mature neurons are mainly composed of the type IV triplet proteins neurofilament light chain (NFL), medium chain (NFM) and heavy chain (NFH) with a thickness of roughly 10nm after assembly. α-internexin and the type III intermediate filament peripherin can also be present within neurofilaments with expression being developmentally regulated: α-internexin and peripherin are expressed within embryonic neurons and during early development. NFL and NFM are also expressed soon after gestation (9-10 days in mice (Cochard & Paulin, 1984)), with NFH beginning to appear as axons mature during myelination. Peripherin can be re-expressed after neuronal injury (Beaulieu, Kriz, & Julien, 2002). Peripherin expression declines in large neurons, but remains a major NF protein in small sensory neurons.

Structurally, NFs retain the classical Head-Rod-Tail trio of domains present in all IFs, with a tail domain of increasing length from NFL to NFH. With the NF triplet proteins, the "tail" C- terminal domain contains many phosphorylation sites (KSP repeats) involved in regulation of interaction with organelles and cytoskeletal elements as well as NF oligomer transport and assembly. Phosphorylation of these sites has also been thought to have a role in maintenance of

axonal radius and growth. The rod domain is a highly conserved α-helix formed of heptad repeats involved in the head to tail assembly to create coiled-coil dimers that themselves assemble into tetramers. The N-terminal head domain contains sites for phosphorylation regulating NF assembly. The exact ratio of each neurofilament type within the completed heteropolymer varies slightly between regions of the nervous system, with the following ratios:

Neurofilaments in general	NFL:NFM:NFH – 4:2:1
Optic nerve of mature CNS	NFL: α-internexin:NFM:NFH – 4:2:2:1
Peripheral nerve neurofilaments (Yuan et al., 2012)	NFL:NFM:Peripherin:NFH – 4:2:1:1

These neurofilament polymers assemble in a non-polarized fashion through end-to-end annealing, being capable of reaching lengths of over 100μm in length in cultured neurons (A. Brown, 1997). This length, combined with the elastic qualities conferred by subunit rearrangement in neurofilaments provide neuronal protection from mechanical stress (H. G. Brown, Troncoso, & Hoh, 1998).

Neurofilament transport and organelle anchoring

Neurofilaments form an interconnected network with other cytoskeletal elements to scaffold and organize organelles in the cytoplasm. For example, they bind the actin microfilament network through plectins and serve as an anchor to the plasmalemma though both plectins and β-spectrins (Macioce et al., 1999). They have a major role in nuclear localization through interactions with linkers of the nucleoskeleton and cytoskeleton (LINC) (Foisner et al., 1988; Morgan et al., 2011). This linker complex connects the intermediate filament network to nuclear lamins. The nuclear outer membrane protein nesprin3 serves to stabilize the perinuclear cytoskeleton and through plectin, interacts with intermediate filaments (Morgan et al., 2011).

Within the intermediate filament network, vimentin has been shown to interact with Golgi through formiminotransferase cyclodeaminase (FTCD) binding, though it remains to be seen if this is recapitulated in NFs (Gao & Sztul, 2001). NFs have an important role in the positioning of the endoplasmic reticulum and axonal mitochondria (Rao et al., 2002) and regulating the dynamics and motility of mitochondria (Gentil et al., 2012). Apart from structural support, it is difficult to ascertain alternative functions of neurofilament due to the difficulty caused by their insolubility in examining direct interactions of NF oligomers. However, yeast two-hybrid experiments have yielded possible signaling activity with NMDA receptors and the ERK2 pathway by α-internexin (Ehlers, Fung, O'Brien, & Huganir, 1998; Karpova et al., 2013).

Neurofilaments and other neurological diseases

Defects in neurofilaments are present in a number of neurological conditions, such as Giant axonal neuropathy (GAN), Charcot-Marie Tooth (CMT) and Amyotrophic Lateral Sclerosis (ALS). The neurofilament structure is of specific interest in these diseases. GAN is a fatal autosomal recessive neurodegenerative disorder that affects both the central nervous system and peripheral nerves, with onset occurring before 5 years (Ganay, Boizot, Burrer, Chauvin, & Bomont, 2011). Caused by loss of gigaxonin protein, GAN progression begins with peripheral symptoms such as muscle weakness and clumsiness that leads to a difficulty with walking, leading to numbness in the extremities, nystagmus and seizures. On a cellular level, loss of gigaxonin function leads to abnormally large axonal swellings containing densely packed intermediate filaments. Axon deterioration leads to peripheral neuropathy. GAN can be assessed with brain MRI, electromyography and a biopsy of peripheral nerves, with genetic testing providing a conclusive diagnostics. Since GAN affects all types of intermediate filaments,

abnormalities can be detected in multiple cell types including fibroblasts cultured from skin biopsies (Pena, 1982). The vimentin intermediate filaments collapse into a juxtanuclear ball.

CMT is an inherited neuropathy characterized by chronic motor-sensory neuropathy accompanied by distal muscle atrophy, weakness, loss of tendon reflexes and foot deformities (Gentil et al., 2012). CMT is a complex disease caused by mutations to a number of proteins, such as peripheral myelin 22, connexin32, MTMR2 among others(Timmerman, Strickland, & Zuchner, 2014). Important to this discussion, CMT variants CMT2E and CMT1F are linked to mutations in NEFL, which promotes aggregation of NFL and disruption of the neurofilament network (Al-Chalabi & Miller, 2003; Zhai, Lin, Julien, & Schlaepfer, 2007).

ALS is a complex motor neuron disease characterized by rapid and highly selective degeneration of both upper and lower motor neurons leading to progressive loss of voluntary muscle function and respiratory failure. While 5-10% of ALS cases are known to be inherited, the majority are sporadic with no known cause. Life expectancy after diagnosis ranges from 6 months to five years. At the molecular level, axons in degenerating motor neurons exhibited accumulations of neurofilaments and peripherin inclusions in both human autopsy samples and transgenic mouse models (Julien, 1997). Additionally, mRNA levels of NFL appear to be depleted in a number of sporadic ALS cases. This is thought to be caused by stoichiometric disruption in the phosphorylation state of NF subunits leading to disorganization of the network. (Gentil, Tibshirani, & Durham, 2015) Also, rates of axonal transport of mitochondria, smooth endoplasmic reticulum and cytoskeletal elements such as actin and tubulin were shown to be significantly decreased in motor neurons exhibiting defective neurofilament architecture (Collard, Cote, & Julien, 1995). This links a critical role in NF structure and transport to other organelles in complex neurological disease.

Neurofilaments and mitochondria

There is a significant role for neurofilaments in the dynamics and motility of mitochondria, as illustrated by mitochondrial fragmentation in models of desmin and vimentin knockdown (Capetanaki, Milner, & Weitzer, 1997). The addition of NF proteins within $SW13^{vim-}$ cells, which completely lack intermediate filament architecture, was shown to cause the development of a reticular mitochondrial network (Gentil et al., 2012). This in indicative of a key role of NF networks in docking mitochondria during stationary time during their transport. Additionally, within cultured motor neurons of $NFL^{-/-}$ mouse spinal cord-dorsal root ganglia (a model that disrupts the NF network), mitochondria demonstrated a decrease in length and rate of fusion. In mice exhibiting a CMT-associated NFL mutation (P8R), mean length of mitochondria was decreased to a similar degree as $NFL^{-/-}$ neurons and formed clusters within axons, contrary to when WT NFL was expressed in motor neurons (Gentil et al., 2012). Because CMT can also be caused by mutation of a mitochondrial pro-fusion protein, MFN2, the link between MFN2 and NFL on mitochondria was studied. In a mouse model exhibiting a CMT-associated mutation (Q333P), rates of fusion were similarly decreased, yet were partially rescued by overexpression of MFN (Gentil et al., 2012). However, MFN2 overexpression in $NFL^{+/+}$ motor neurons yielded no significant change in rates of fusion, indicative of the presence of distinct mechanisms responsible for mediation of mitochondrial length and stability from both pro-fusion proteins and intermediate filament proteins (Gentil et al., 2012).

Chapter 2: Hypothesis and rationale

Hypothesis and Specific Aims

Hypothesis:

Sacsin loss of function mutations are associated with mitochondrial dysfunction and linked to abnormalities in the intermediate filament network.

Rationale:

Mitochondrial defects have been observed in a number of ARSACS models and intermediate filaments are important for organizing the intracellular space. Both dysfunction in the cytoskeletal network and mitochondrial physiology have been linked to neurodegenerative diseases such as ALS and Charcot-Marie Tooth (Barry, Millecamps, Julien, & Garcia, 2007; Brownlees et al., 2002; Gentil & Cooper, 2012; Gentil et al., 2012; Miller et al., 2002; Tradewell et al., 2009). The highly interconnected nature of the two presents a promising area of study in assessing ARSACS molecular pathology. The chaperone activity of sacsin as well as the presence of defective mitochondrial morphology in its absence could indicate a potential role for sacsin acting as a chaperone to proteins critical to proper function of mitochondria, intermediate filaments or both.

In primary sacsin knockdown hippocampal cultures, fewer mitochondria were detected in dendrites compared to wild-type cultures (Girard et al., 2012). The number of dendrites surrounding the cell body was also decreased. In motor neurons from $Sacs^{-/-}$ dissociated spinal cord-dorsal root ganglion cultures, immunocytochemical labeling of NFH revealed bundling of neurofilaments in the dendrites, and mitochondria had a longer mean length (Lariviere et al., 2014). Additionally, siRNA-mediated sacsin knockdown in SH-SY5Y human neuroblastoma

cells significantly decreased mitochondrial membrane potential, as determined by TMRM labeling, further supporting a potential defect in oxidative phosphorylation (Girard et al., 2012).

Neurofilament pathology is prominent in ARSACS. In patient brains and in ARSACS knockout mice (*Sacs*$^{-/-}$), neurofilament bundles are prominent the somatodendritic region of neurons (Lariviere et al., 2014). Interestingly, immunohistochemical analysis demonstrated that the bundles were enriched in non-phosphorylated NFH, further demonstrating the importance of altered stoichiometric balance at the neurofilament level. The connection between cytoskeletal and mitochondrial architecture in neurological disease has been well characterized (Gentil et al., 2012).

The purpose of this study was to further evaluate mitochondrial involvement in ARSACS and assess the relationship to neurofilament bundling, using two experimental models: 1) spinal cord cultures from Sacs$^{-/-}$ mice and 2) fibroblasts derived from skin biopsies of ARSACS patients. This study measured:

1) Mitochondrial length

2) mtRNA transcription efficiency

3) Abundance of oxidative phosphorylation machinery

4) Morphology and localization of the intermediate filament network

Specific aims:

1. **Specific Aim** 1: To further assess the mitochondrial phenotype using two experimental models of ARSACS: embryonic spinal cord-dorsal root ganglion (DRG) cultures from *Sacs*$^{-/-}$ mice and fibroblasts derived from ARSACs patients (c. del8844T) compared to controls (cultures prepared from wild type mice and fibroblasts derived from healthy individuals, respectively).
2. **Specific Aim 2**: Further assess the intermediate filament phenotype in ARSACS models, with particular reference to organization of mitochondria and other organelles and comparison to another disorder of intermediate filament organization, GAN.

Experimental Approach

Specific Aim 1: To further assess the mitochondrial phenotype using two experimental models of ARSACS: embryonic spinal cord-dorsal root ganglion (DRG) cultures from *Sacs*$^{-/-}$ mice and fibroblasts derived from ARSACs patients (c. del8844T) compared to controls (cultures prepared from wild type mice and fibroblasts derived from healthy individuals, respectively).

1.1. Measure the length of mitochondria in dendrites of motor neurons in mouse dissociated spinal cord-DRG cultures and in cultured fibroblasts.

In order to label mitochondria, three methods were used as needed: immunocytochemistry against mitochondrial markers such as TOM20, mitochondrial labelling using MitoTracker DeepRed and adenoviral transduction to express mitochondrially targeted CFP (*AV-CMV-OCT-CFP*). The mean length as well as the overall distribution of mitochondrial lengths between ARSACS and control cells were compared.

1.2. Determine if loss of sacsin function causes defects in mitochondrial RNA transcription and RNA granule colocalization.

Colocalization of new mtRNA transcripts with RNA granules was assessed by incorporation of the uridine analogue, BrU, followed by immuno-detection using antibodies against BrU (anti-BrU) as well as RNA granules (anti-FASTKD2).

1.3. Determine if loss of sacsin function alters the abundance of respiratory chain complexes.

This was assessed in the fibroblast model, using blue native-polyacrylamide gel electrophoresis (BN-PAGE) to characterize the assembly of the oxidative phosphorylation machinery in isolated mitochondria.

Specific Aim 2: Further assess the intermediate filament phenotype in ARSACS models, with particular reference to organization of mitochondria and other organelles and comparison to another disorder of intermediate filament organization, GAN.

2.1. Determine how altered intermediate filament organization affects distribution of the Golgi, endoplasmic reticulum (ER) and nucleus in ARSACS.

Intermediate filament organization was evaluated by immunocytochemistry; anti-NFH in motor neurons and anti-vimentin in fibroblasts. ER was visualized by anti-KDEL, Golgi by anti-GM130 and the LINC complex linking intermediate filaments to the nucleus by anti-nesprin3 and anti-emerin, members of the LINC complex at the outer and inner nuclear membrane, respectively.

*2.2***:** *Determine the specificity of the phenotype to ARSACS by comparing to another disorder characterized by intermediate filament bundling, Giant Axonal Neuropathy (GAN).*

The parameters with abnormal measurements in ARSACS fibroblasts were measured in fibroblasts derived from GAN patients to determine if these changes are a common result of intermediate filament bundling.

Chapter 3: Materials and methods

3.1: Cell culture

3.1.1. Sacs$^{-/-}$ mouse line

Sacs$^{-/-}$ mice were generated in the laboratory of Dr. Bernard Brais by replacement of exon 10 with an IRES-βGal cassette (Girard et al., 2012). Loss of sacsin expression was confirmed by Western blot.

3.1.2. Preparation of mouse primary dissociated spinal cord-DRG cultures

Dissociated spinal cord-DRG cultures were prepared from embryonic day 13 (E13) C57Bl6 or *Sacs*$^{-/-}$ mice on the same background (C57Bl6). Spinal cords with attached DRGS were harvested and placed in a 60 mm dish containing 1 mL of dissecting medium (PBS, sucrose, dextrose and HEPES). Post-harvest, spinal cords were minced by scalpel and dissociated with the addition of 2 mL of dissecting solution and 300 µL of 2.5% trypsin solution. After 30 minutes at 37^{o}C, cells were transferred to modified N3 medium (Dulbecco's minimum essential medium supplemented with 5g/L glucose, 3% horse serum, 10 µg/ml bovine serum albumin, 26ng/ml selenium, 20ng/ml triiodothyronine, 10 µg /ml insulin, 200 µg /ml transferrin, 32 µg /ml putrescine, 9.1 ng/ml hydrocortisone, 13ng/ml progesterone, and 5 ng/ml nerve growth factor) in order to neutralize trypsin. The spinal cords were then further dissociated using a Pasteur pipette into N3 medium. Cells were plated in 12-well culture dishes containing 15mm glass coverslips coated with Poly-D-lysine and Matrigel basement membrane matrix. Cells were plated at a density of 375,000 per well. Cells were maintained in N3 and at day 4-6. Once cultures reached confluence, they were treated with 1.4 µg/ml cytosine- β -D-arabinoside (CAF) in N3 medium for 2 days to inhibit mitosis of non-neuronal cells. Cultures were maintained in N3 medium at 37^{o}C in 5% CO_2 and fed twice a week by replacing half of the medium.

3.1.3. Human fibroblast cultures

Human fibroblast strains (McGill University Health Centre (MUHC) Cell Bank) were immortalized (in the Shoubridge lab) and used in this study: healthy controls (MCH046, MCH064 and MCH074); ARSACS patients (MCH087 and MCH366) with the c.8844delT French Canadian mutation, and a GAN patient (WG791). Cryopreserved fibroblasts were stored in 10% dimethylsulfoxide (DMSO), 40% fetal bovine serum (FBS) and 50% complete medium (Dulbecco's minimum essential medium (DMEM), 10% FBS, 1% Penicillin/Streptomycin). Cells were cultured by plating 3 x 10^5 to 1 X 10^6 in 10 cm culture dishes using DMEM with 10% FBS. In 12-well dishes, cells were plated on 15 mm glass coverslips at 2.5 x 10^4 per well. For splitting, cells were incubated in 2 mL 2.5% trypsin for 5 minutes at 37^{o}C. 8 mL of complete medium are then added to neutralize trypsin.

3.2. Experimental methods

3.2.1. Mitochondrial labeling

Mitochondria were labeled by expressing a genetically encoded fluorescent marker targeted to mitochondria using the signal sequence of ornithyl-carboxytransferase. Because of the high efficiency of transduction in primary cells, an adenoviral vector was used to express mitochondrially targeted CFP (*AV-CMV-OCT-CFP*). Cells were treated with a solution of 1 x 10^6 PFU adenovirus/mL of medium for 24 hours prior to fixation. Mitochondria were alternately labelled with MitoTracker DeepRed (ThermoFisher Catalog number M22426) for 1 hour before fixation, or by immunocytochemistry using anti-TOM20. Mitochondrial lengths in fibroblasts and primary motor neurons were measured with ImageJ software (Schindelin et al., 2012).

3.2.2. 5-Bromouridine (BrU) incorporation

Detection of newly transcribed mitochondrial RNA was accomplished by incorporation of the uridine analogue BrU, which is detectable by a monoclonal anti-BrdU antibody (listed below). Both fibroblasts and neuronal culture were incubated for 30 minutes with 5 mM BrU diluted in culture medium. Cells were then washed and fixed for immunocytochemistry (protocol below).

3.2.3. Immunocytochemistry for cultured cells

Cells were fixed in 3% paraformaldehyde (PFA) in PBS for 10 minutes and permeabilized in 0.5% Triton-X in phosphate-buffered saline (PBS) for 10 minutes followed by a subsequent fixation for 2 minutes. Cells were then blocked by incubating in 5% equine serum in PBS at RT for 30 minutes. Blocking was followed by incubations with primary and secondary antibody solutions diluted in blocking buffer for 45 minutes and 30 minutes, respectively, each followed by three 5 minute washes. Coverslips were then briefly dried and mounted on glass microscope slides (Fisher Scientific, ON, Canada) using Immumount (Thermoscientific, MI, USA).

3.2.4. Sample preparation and Blue-Native PAGE

Sample preparation, including crude mitochondrial fraction

Cultured human fibroblasts were trypsinized and centrifuged in a 15 mL Falcon tube at 1000 x G for 5 minutes before they were washed once with PBS. Following another centrifugation at 1000 x G for 5 minutes, cells were resuspended in cold PBS (0.5 ml PBS per 10 cm plate, 1 ml PBS for a 15 cm plate). Protein concentration was determined using the Bradford protein assay. Following another wash step (centrifugation at 1000 x G for 5 minutes), and the

sample was resuspended in PBS to a final concentration of 5 mg protein/ml and transferred to a 2 mL Eppendorf tube. Digitonin (4mg/mL) was added at a 1:1 ratio to cell suspension and incubated on ice for 5 minutes for a final concentration of cells of 2.5 mg/mL and a final digitonin concentration of 2 mg/mL (digitonin/protein ratio of 0.8). After incubation, PBS was added to final volume of 2 mL before a centrifugation step at 10 000 x G for 10 minutes. After discarding supernatant, sediment (membranes) were resuspended in MB2 (0.5 ml 3xGB, 0.5 ml 2M Aminocaproic acid, 4µl 500mM EDTA**)** buffer at a volume equal to half of the volume of PBS used to achieve a protein concentration of 5mg/mL. lauryl maltoside (LM, dodecyl malthoside 10%) was added to a final concentration of 1% and incubated on ice for 15 minutes. Mitochondria were centrifuged at 20 000 x G for 20 minutes, with the supernatant (mitochondria) being placed in a new Eppendorf tube and quantified by Bradford protein assay. Sample buffer (750 mM Aminocaproic acid, 5% Serva Blue G) was added to purified mitochondria with a volume of ½ of lauryl maltoside used. Samples were frozen at -20 °C until used.

Blue-Native PAGE: Preparation of gel and electrophoresis

Using a Miniprotean Bio Rad apparatus with 1 mm spacers and combs, a 6-15% acrylamide gradient native gel was prepared according to standard protocol. 5 mL of 6% and 15% separating gel mixture was prepared according using 3x GLB (1.5M aminocaproic acid, 150 mM Bis-tris, pH 7.0), acrylamide/bisacrylamide mix (48% acrylamide, 1.5% bisacrylamide (99.5T, C) , 10% glycerol, 0.05% ammonium persulfate and 0.05% TEMED (Tetramethylethylenediamine).

Tubing and the bottom 1 cm of the glass sandwich cassettes were filled with water. The front reservoir of the gradient mixer was filled with 2.8 mL of 6% mixture solution and the rear reservoir was filled with 2.3 mL of 15% mixture solution. The gel cassette was filled by underlying the gel under water using peristaltic pump. Following gel polymerization, the gel surface was washed with 1x gel buffer. 2.5 mL of stacking mixture was prepared and added and a 15 well comb was inserted. After polymerization of the stacking layer, the comb was removed and the wells were washed with 1x GB. Spaces in wells were filled with blue cathode buffer and 20 µg protein of each sample was layered under buffer into wells, ensuring that sample volumes did not exceed 20 µl/well.

Gel cassettes were placed into apparatus and upper and lower reservoirs were filled with blue cathode buffer (Cathode buffer cont. 0.02% Serva Blue G (SBG)) and anode buffer (50 mM Bis-tris, pH 7.0), respectively. The gel was run for 15 min at 40V, then at 80V until the dye reached 2/3 of the gel. Following this, blue cathode buffer was replaced with transparent cathode buffer (15 mM Bis-tris, 50 mM Tricine, pH 7.0). Electrophoresis continued until the dye front reached the bottom of the plate. The gel was removed from between the plates and underwent semi-dry transfer for one hour at 0.08 mA in a Pharmacia Biotech semi-dry transfer cell.

3.2.5. Statistics

Statistical significance was defined at $p<0.05$. An unpaired t-test is used to directly compare two experimental conditions.

3.3. Antibodies used

Primary antibodies:

Mouse anti-BrdU (Roche, 11 296 736 001)	1:200
Rabbit anti-TFAM (ProteinTech, 19998-1-AP)	1:100
Rabbit anti-FAST-KD2 (Amersham, RPN1194)	1:100
Mouse anti-GRSF1 (Sigma-Aldrich)	1:500
Mouse anti-Cytochrome C (PharmaGen)	1:1000
Rabbit anti-TOM20 (Santa Cruz, 11415)	1:250
Mouse anti-DNA (PROGEN Biotechnik GmbH)	1:500
Mouse anti-NFL (Chemicon)	1:300
Mouse anti-Vimentin (Chemicon)	1:300
Mouse anti-Nesprin-3 (Sigma-Aldrich)	1:300
Mouse anti-Emerin (Sigma-Aldrich)	1:300
Mouse anti-GM130 (Abcam)	1:500
Rabbit anti-GM130 (Abcam)	1:500
Rat anti-KDEL (Abcam)	1:500

Secondary Antibodies:

Donkey anti-mouse Cy2 (Rockland)	1:300
Donkey anti-mouse Cy3 (Jackson)	1:300
Donkey anti-rabbit Cy2 (Jackson)	1:300
Donkey anti-rabbit Cy3 (Jackson)	1:300
Donkey anti-mouse Cy5 (Jackson)	1:300
Donkey anti mouse YFP	1:300
Goat anti rabbit YFP	1:300

Chapter 4: Results

4.1. Further assess the mitochondrial phenotype using two experimental models of ARSACS: embryonic spinal cord-dorsal root ganglion (DRG) cultures from Sacs$^{-/-}$ mice and fibroblasts derived from ARSACs patients (c. del8844T) compared to controls (cultures prepared from wild type mice and fibroblasts derived from healthy individuals, respectively).

4.1.1. Measure the length of mitochondria in dendrites of motor neurons in mouse dissociated spinal cord-DRG cultures and cultured fibroblasts

Dr. Benoit Gentil in the Durham lab previously demonstrated mitochondrial elongation in axons of motor neurons of dissociated spinal cord-DRG cultures prepared from Sacs$^{-/-}$ mice, but mitochondrial fragmentation in DRG sensory neurons(Lariviere et al., 2014). To assess and confirm a mitochondrial length phenotype in motor neuron dendrites, several mitochondrial labelling techniques were used. Adenoviral transduction with OCT-CFP, Mitotracker DeepRed incubation and immunocytochemistry all labelled mitochondria equally well (Figure 2). The flat morphology of motor neuron dendrites facilitates visualization of the mitochondrial network. Mitochondrial measurements were taken using cells at 3 and 5 weeks of *in vitro* age in both *Sac* $^{-/-}$ and *Sacs*$^{+/+}$ cultures. Motor neurons mature over 3 weeks in wild-type cultures, but with a 2 week delay in maturation in *Sac* $^{-/-}$ cultures (Lariviere et al., 2014). Mean mitochondrial length in the dendrites of both 3- and 5-week-old motor neurons was increased in *Sac* $^{-/-}$ motor neurons and reached statistical significance ($p < 0.05$, unpaired t-test, (Figure 3A and 3B). The distribution of mitochondrial lengths was plotted (Figure 3C and 3D) and shows the shift in mitochondrial length distributions with loss of sacsin: in 3 week-old *Sacs*$^{+/+}$ dendrites the highest proportion of mitochondria had lengths of 2-2.25 μm, with roughly 10% of mitochondria

measured in that range. In comparison, in 3 week-old *Sacs*$^{-/-}$ motor neurons, approximately 8% of mitochondria distributed to each 2.5-2.75 and 2.75-3 μm (total 16%) In 5 week-old *Sacs*$^{-/-}$ cultures, the peak distribution (approximately 14%) of mitochondria were in the 2.25-2.5 μm range, while in *Sacs*$^{+/+}$ cultures, 13.5% of mitochondria were between 2.5-2.75 μm in length.

In order to compare mitochondrial length in ARSACS patient fibroblasts to the changes seen in *Sacs*$^{-/-}$ primary cultures, mitochondrial lengths were measured using the same labelling techniques mentioned above. In healthy fibroblasts, the mean mitochondrial length for the three patient lines (MCH046, MCH064 and MCH074) was 2.31, 2.57 and 2.62 μm, respectively. In the ARSACS patient lines MCH087 and MCH366, mean mitochondrial lengths were 3.42 and 3.09 μm, respectively. The difference between ARSACS and healthy patient mitochondrial length is statistically significant ($p < 0.01$, unpaired t-test, Figure 4A). In terms of distribution of mitochondrial lengths, pooled mitochondrial length measurements from the healthy fibroblast cells were most highly distributed between 1.5-1.75 um, with approximately 10% of all measured mitochondria in this bin. By comparison, the length range with the highest distribution in ARSACS patients was approximately 8% at a length of 2.25-2.5 μm and from 2.75-3 μm (Figure 4B).

4.1.2. Determine if loss of sacsin function causes defects in mitochondrial RNA transcription and RNA granule colocalization

In order to characterize mtRNA transcription and assess localization of nascent RNA to granules, incorporation of the brominated uridine analogue, BrU, was assessed in fibroblasts. Cells were incubated with MitoTracker DeepRed and underwent a 30 minute incubation with 5 mM BrU. Following fixation and immunolabeling with anti-BrU and anti-FASTKD2 antibodies,

cells were imaged by confocal microscopy using an Olympus Spinning Disk microscope. Co-localization of labelled BrU with mitochondria was first confirmed through line profile intensity measurement (representative image in Figure 6) through use of the ImageJ colocalization plugin. This generates a pixel co-localization map (Figure 7C), a scatterplot (Figure 7D), and calculates the Pearson's correlation coefficient as well as Manders co-localization coefficients for BrU overlap with FASTKD2 and vice versa (M1 and M2). As demonstrated in Figure 7E, there is no statistically significant change in either the co-localization or correlation coefficients when comparing ARSACS patient fibroblasts with healthy controls.

BrU incorporation was also attempted in motor neurons of spinal cord-DRG cultures. However, labelling of BrU and FASTKD2 with their respective antibodies appeared less specific, leading to more background signal. It was therefore impossible to generate a co-localization map through ImageJ in order to quantify Pearson's correlation coefficient or Manders co-localization coefficients.

4.1.3. Determine if loss of sacsin function alters the abundance of respiratory chain complexes

To ascertain if respiratory chain complex assembly is defective in ARSACS, BN-PAGE analysis was performed on mitochondria isolated from fibroblasts. BN-PAGE allows for the electrophoretic separation of the assembled respiratory chain complexes. . This analysis was not performed using the dissociated spinal cord-DRG cultures because they do not comprise a single cell type, but a mix of glial and neuronal cell types. This makes it impossible to draw conclusions about what occurs in specific neuronal types, including motor neurons.

A crude mitochondrial fraction was prepared from control and ARSACS fibroblasts and 20 µg of protein were run on the native gel. Following semi-dry transfer and blocking, membranes were blotted with antibodies against Complexes I, II, III, IV and V. By visual inspection of the developed films, there was no difference in protein abundance or electrophoretic mobility for any of the targeted complexes (Figure 8).

4.2. Further assess the intermediate filament phenotype in ARSACS models, with particular reference to organization of mitochondria and other organelles

4.2.1. Determine how altered intermediate filament organization affects distribution of the Golgi, endoplasmic reticulum (ER) and nucleus in ARSACS

The formation of neurofilament bundles is characteristic of ARSACS patients and ARSACS mice. To replicate this in dissociated spinal cord-dorsal root ganglion (DRG) cultures and human fibroblasts, immunocytochemistry was performed using antibodies against the specific intermediate filament protein for each cell type, namely NFH for motor neurons and vimentin for fibroblasts. NFH labeling revealed NF bundles in motor neurons of *Sac* $^{-/-}$ mouse cultures coursing through the dendrites and within the cell body. In healthy fibroblasts, vimentin forms a filamentous networks across the cell (Figure 5). ARSACS patient fibroblasts exhibiting vimentin-positive bundles surrounding the nucleus and radiating out in the cytoplasm. In many cells, the filament bundles were collapsed in the juxtanuclear region (Figure 5).

Dr. Benoit Gentil of the Durham Lab previously demonstrated that in neurons of *Sacs*$^{-/-}$ mouse spinal cord-DRG cultures, there was eccentric positioning of the nucleus. This raised questions regarding the role of neurofilament bundling in maintenance of nuclear placement: The

cytoskeletal network positions the nucleus through a protein complex called the "linkers of the nucleoskeleton and cytoskeleton" (LINC complex). Briefly, intermediate filaments interact with plectin, which itself binds the nuclear outer membrane (OM) protein nesprin3. Nesprin3 is embedded in the nuclear outer membrane, and connected to inner-membrane (IM)-bound emerin. Emerin is anchored to nuclear lamins. Through the LINC complex, intermediate filaments stabilize the cytoskeleton around the nucleus.

In order to determine whether or not loss of sacsin function had a direct effect on the LINC complex, the localizations of OM protein nesprin3 and IM protein emerin were examined. Dr. Benoit Gentil performed immunocytochemistry in neurons of *Sacs*$^{-/-}$ mouse spinal cord-DRG cultures. Emerin immunolabeling demonstrated the name nuclear localization in both *Sacs*$^{-/-}$ and controls. Nesprin3 immunolabeling demonstrated a mild abnormality in its perinuclear localization, with some colocalization with neurofilaments. In ARSACS and control fibroblasts, emerin immunolabeling showed the expected nuclear localization in both (Figure 9). Nesprin3 immunoreactivity was localized around the nucleus as well as some punctate distribution in the cytoplasm (nesprin3 also associates with other membranous organelles) in control cells; however, in ARSACS cells, the nuclear labelling was disrupted and nesprin3 colocalized very strongly with vimentin aggregates (Figure 10) (Rao et al., 2011).

In addition to acting on nuclear positioning, intermediate filaments have a general role in organelle localization. The Golgi apparatus has been directly functionally linked to vimentin networks and localization (Gao & Sztul, 2001). Furthermore, intermediate filaments, specifically NFL, interact with the endoplasmic reticulum via myosin Va. Myosin Va is a subclass of molecular motor proteins responsible for trafficking membrane-bound vesicles, mitochondria and ER cargos (Rao et al., 2011). Griscelli disease type 1 is an autosomal recessive disease

caused by loss of function of Myosin Va. Symptoms include hypopigmentation, immunodeficiency and severe neurological defects (Miyata et al., 2011). Furthermore, NFL and Myosin Va loss has been associated with ER reduction in mouse axons. Immunolabeling of Golgi and endoplasmic reticulum markers was used to interrogate the effect of sacsin loss function on organelle organization. Dr. Gentil's previous work in neurons of *Sacs*$^{-/-}$ mouse spinal cord-DRG cultures demonstrated no change in localization or morphology of the Golgi apparatus with abnormal distribution of the endoplasmic reticulum (Data not shown). In fibroblasts derived from ARSACS patients, Golgi immunolabeling with anti-GM130 antibody showed no demonstrative difference in localization (Figure 11). However, labelling of the endoplasmic reticulum demonstrated that juxtanuclear vimentin bundles displaced the ER (Figure 12).

4.2.2. Determine the specificity of the phenotype to ARSACS by comparing to another disorder characterized by intermediate filament bundling, Giant Axonal Neuropathy (GAN).

Both intermediate filament bundling and altered mitochondrial morphology were consistent features in both motor neurons cultured from Sacs$^{-/-}$ mice and in ARSACS patients' fibroblasts with the del8844T mutation. Other studies have linked changes in mitochondrial length and transport as a secondary effect of disrupting intermediate filaments (Gentil et al., 2012). To determine if mitochondrial changes occurred independent of intermediate filament abnormalities or were a secondary result, measurements were compared in fibroblasts from a patient with GAN, another disease with primary involvement of intermediate filament organization.

The disruption of intermediate filament organization in ARSACS and GAN fibroblasts is similar, but more pronounced in GAN. GAN fibroblasts show larger bulbar juxtanuclear

aggregates of vimentin (Figure 13, 14, 15, 16). In order to ascertain whether or not vimentin aggregates in GAN cells affected mitochondrial length, measurements were taken in cells with and without vimentin bundles (Figure 17). Compared to healthy patient controls, there was no significant difference in mitochondrial length in GAN fibroblasts, either in general or when categorized according to presence or absence of prominent vimentin bundles. With regards to mitochondrial length distribution, there was no significant difference in distribution pattern of mitochondrial lengths.

In order to further characterize GAN fibroblasts as a comparison to ARSACS, immunocytochemistry was performed to assess localization and morphology of nuclear membrane proteins and organelles. In GAN cells, emerin maintained perinuclear localization comparable to controls (Figure 13). Nesprin3 in GAN fibroblasts was highly mislocalized to vimentin accumulations instead of the nucleus (Figure 14). Similar to ARSACS fibroblasts, ER was displaced by vimentin bundles while the Golgi apparatus remained unchanged (Figure 15, Figure 16).

In summary, the changes in mitochondria with regards to increased length are unique to ARSACS. However, the rearrangement of nesprin3 and displacement of the endoplasmic reticulum are common and secondary to disorganization in the intermediate filament network.

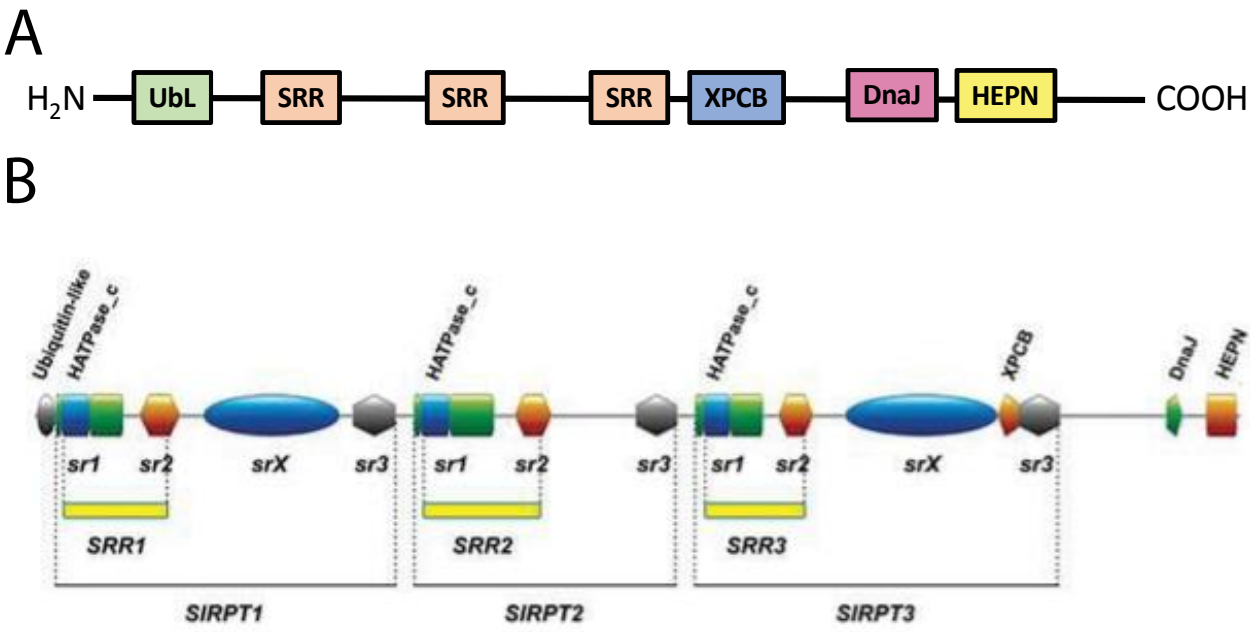

Figure 1: Sacsin protein structure: Sacsin has 7 total domains. (A) Simplified schematic of sacsin. Starting from the N-terminal: UBL domain, 3 sacsin repeating region (SRR) domains, XPCB domain, DnaJ domain and HEPN domain. (B) Detailed schematic including Sacsin Internal RePeaTs (*SIRPTs*) and subrepeats 1 (*sr1*), 2 (*sr2*), 3 (*sr3*), and X (*srX*) within *SIRPTs* are indicated: Domain localization*SIRPT1* (amino acids 84–1,374), *SIRPT2* (1,444–2,443), *SIRPT3* (2,512–3,896), *SIRPT1–sr1* (84–339), *SIRPT1–sr2* (400–557), *SIRPT1–sr3* (1,212–1,374), *SIRPT1–srX* (644–1,162), *SIRPT2–sr1* (1,444–1,747), *SIRPT2–sr2*(1,826–1,968), *SIRPT2–sr3* (2,287–2,443), *SIRPT3-sr1* (2,512–2,768), *SIRPT3–sr2* (2,826–2,960), *SIRPT3–sr3* (3,736–3,896), *SIRPT3–srX* (3,081–3,659). Figure and figure legend adapted from (Romano et al., 2013)

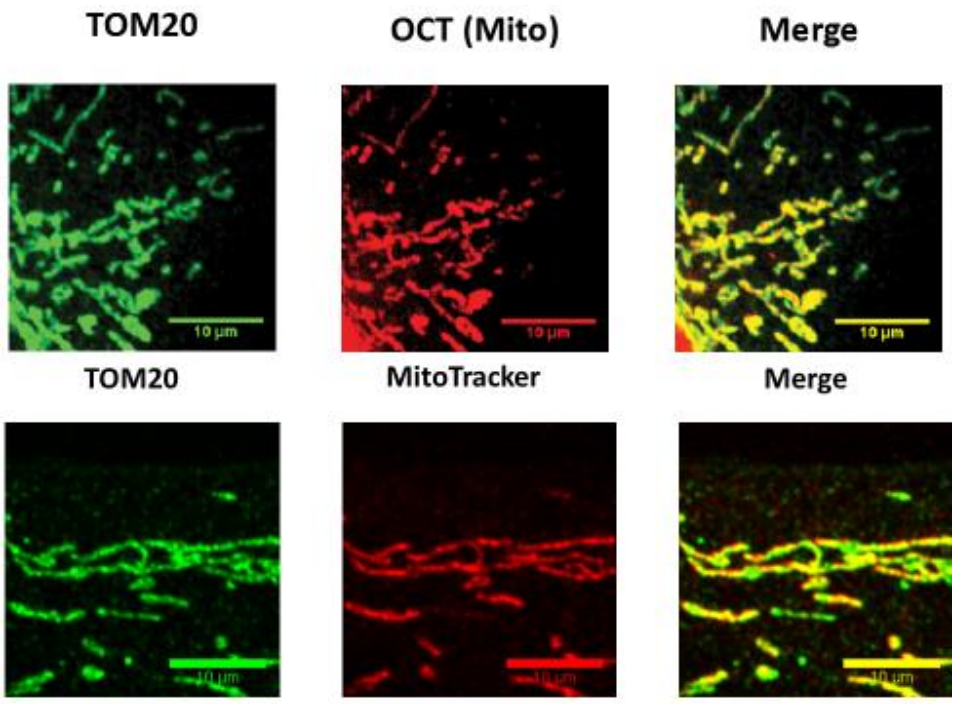

Figure 2: Three mitochondrial labelling methods as shown in cultured human fibroblasts: Immunocytochemical labeling with a TOM20 antibody, adenoviral transduction with AV-CMV-OCT-CFP and labelling with MitoTracker DeepRed.

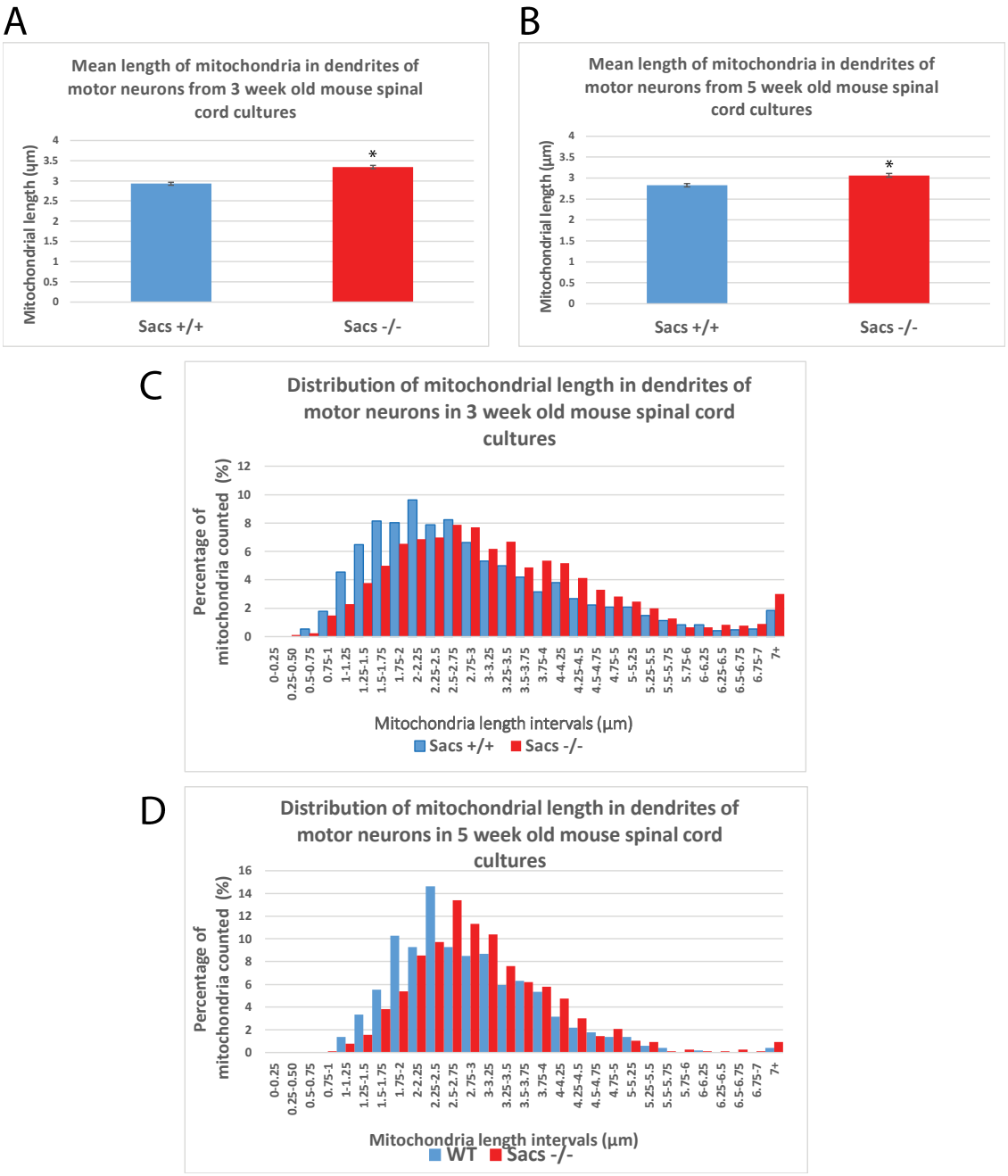
A
Mean length of mitochondria in dendrites of motor neurons from 3 week old mouse spinal cord cultures
Mitochondrial length (µm)
Sacs +/+
Sacs -/-
B
Mean length of mitochondria in dendrites of motor neurons from 5 week old mouse spinal cord cultures
Mitochondrial length (µm)
Sacs +/+
Sacs -/-
C
Distribution of mitochondrial length in dendrites of motor neurons in 3 week old mouse spinal cord cultures
Percentage of mitochondria counted (%)
Mitochondria length intervals (µm)
Sacs +/+
Sacs -/-
D
Distribution of mitochondrial length in dendrites of motor neurons in 5 week old mouse spinal cord cultures
Percentage of mitochondria counted (%)
Mitochondria length intervals (µm)
WT
Sacs -/-

Figure 3.

Figure 3: Dendritic mitochondrial length in cultured primary motor neurons of *Sacs*$^{-/-}$ mice are longer than in *Sacs*$^{+/+}$ mice. (A) Measurements of mean length of dendritic mitochondria in three week-old motor neurons. Asterisks indicate significance compared to *Sac* $^{+/+}$ control ($p<0.05$; two-tailed t-test). (B) Measurements of mean length of dendritic mitochondria in five week-old motor neurons. Asterisks indicate significance compared to Sacs$^{+/+}$ control ($p<0.05$; two-tailed t-test). (C) Distribution of mitochondrial lengths in three week-old motor neurons from *Sacs*$^{-/-}$ and *Sacs*$^{+/+}$ mice. Mitochondrial lengths were binned into 0.5-μm intervals. (D) Distribution of mitochondrial lengths in five week-old motor neurons from *Sacs*$^{-/-}$ and *Sacs*$^{+/+}$ mice. Mitochondrial lengths were binned into 0.25-μm intervals.

A

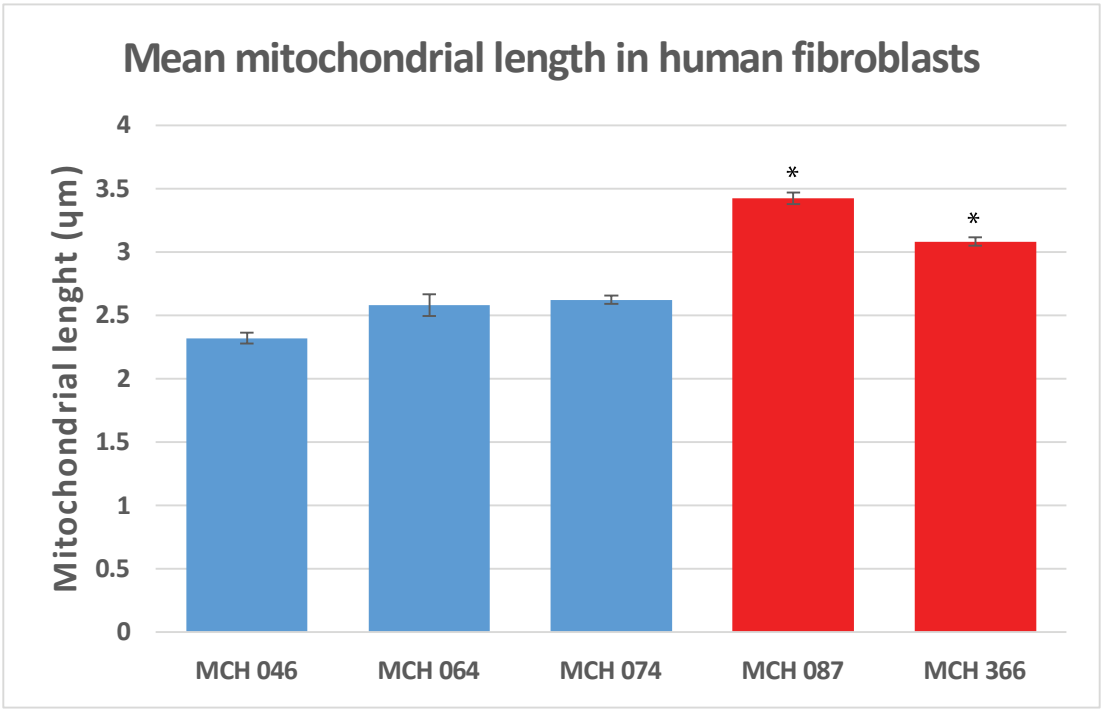
Mean mitochondrial length in human fibroblasts
Mitochondrial lenght (µm)
4
3.5
3
2.5
2
1.5
1
0.5
0
*
*
MCH 046
MCH 064
MCH 074
MCH 087
MCH 366

B

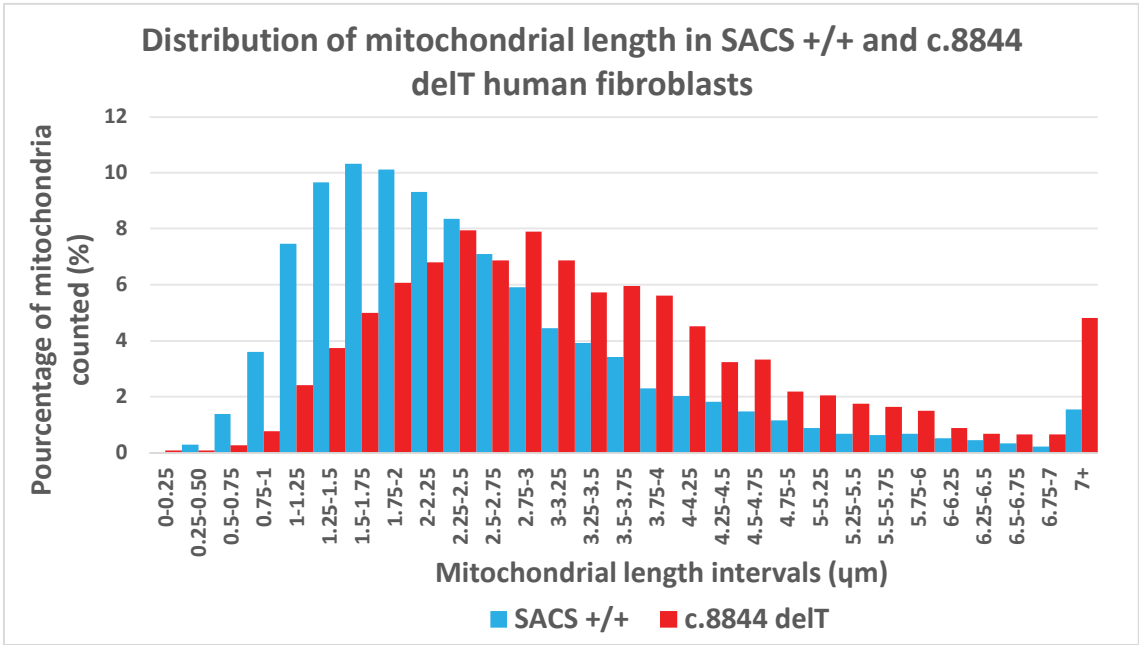
Distribution of mitochondrial length in SACS +/+ and c.8844 delT human fibroblasts
Pourcentage of mitochondria counted (%)
12
10
8
6
4
2
0
0-0.25
0.25-0.50
0.5-0.75
0.75-1
1-1.25
1.25-1.5
1.5-1.75
1.75-2
2-2.25
2.25-2.5
2.5-2.75
2.75-3
3-3.25
3.25-3.5
3.5-3.75
3.75-4
4-4.25
4.25-4.5
4.5-4.75
4.75-5
5-5.25
5.25-5.5
5.5-5.75
5.75-6
6-6.25
6.25-6.5
6.5-6.75
6.75-7
7+
Mitochondrial length intervals (µm)
SACS +/+
c.8844 delT

Figure 4.

Figure 4: Mitochondrial length in cultured human ARSACS fibroblasts are longer than in those from healthy patients. (A) Measurements of mean length of dendritic mitochondria in human fibroblasts from three control subjects (MCH046, MCH 064 and MCH074) and two ARSACS patients (MCH087 and MCH366). Asterisks indicate significance compared to control ($p<0.05$; two-tailed t-test). (B) Distribution of lengths of dendritic mitochondria in human fibroblasts from three pooled control subjects (MCH046, MCH 064 and MCH074) and two pooled ARSACS patients (MCH087 and MCH366). Mitochondrial lengths were binned into 0.25-μm intervals.

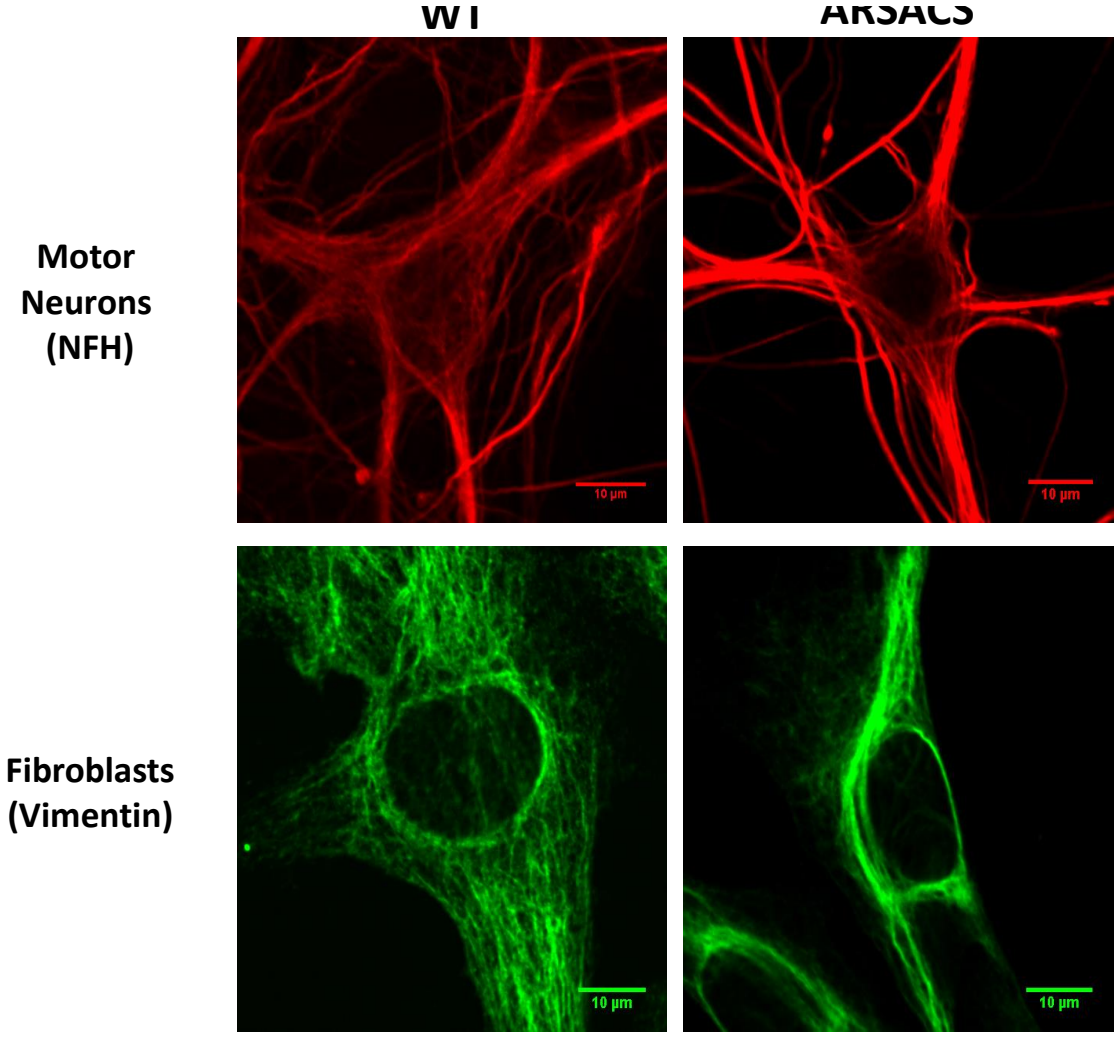

Figure 5: Human ARSACS patient fibroblasts display intermediate filament bundling comparable to neurofilament bundling seen in cultured primary motor neurons of *Sacs*$^{-/-}$ mice. Immunocytochemistry using antibodies against neurofilament heavy chain protein (mouse primary motor neurons) and vimentin (cultured fibroblasts).

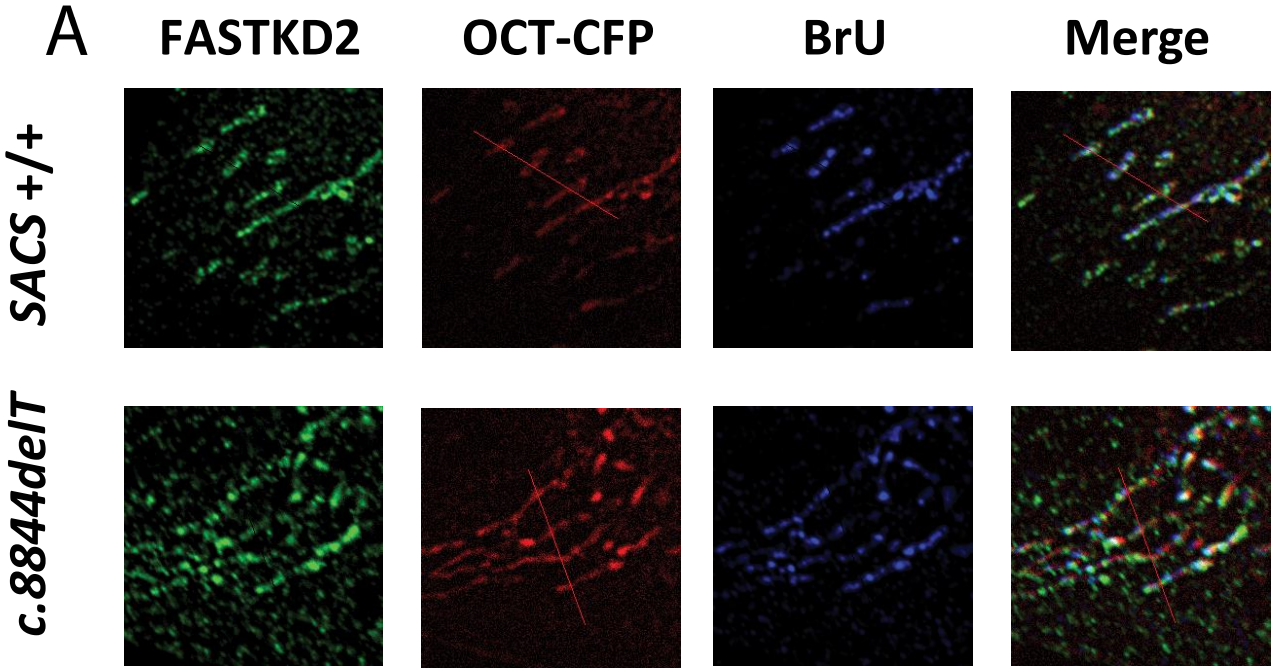

Figure 6: Representative confocal image of cultured human fibroblasts transfected with OCT-CFP, labeled with BrU, and immunolabeled with anti-FASTKD2 and anti-BrU antibodies. Merged image shows colocalization of FASTKD2 and BrU within mitochondria.

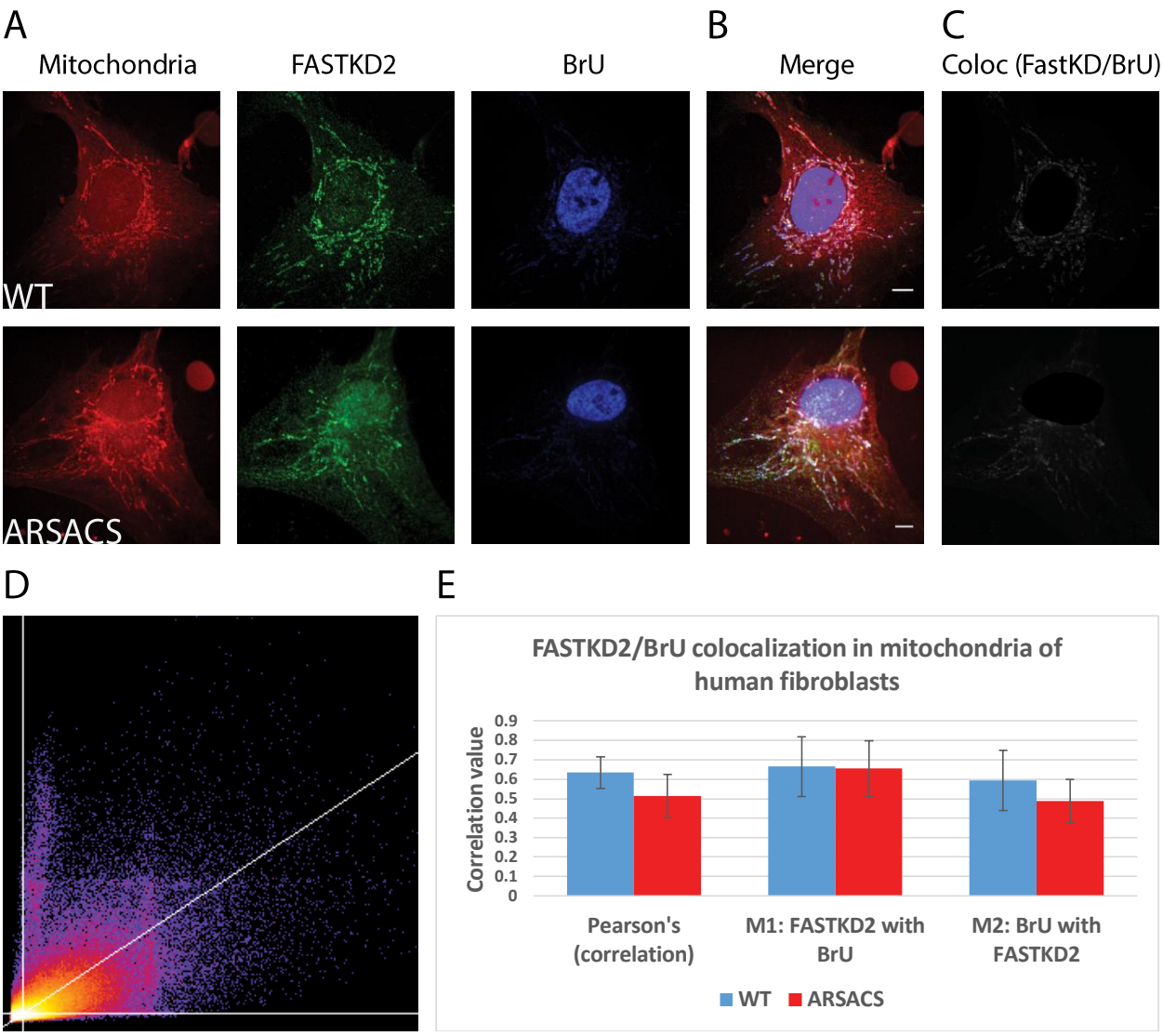

Figure 7: Representative images of colocalization analysis using ImageJ software. Colocalization of non-nuclear intensity of BrU and FASTKD2 signal. Confocal image split by channel (A) and merged (B) of fibroblast transfected with OCT-CFP, labelled with BrU, and immunolabeled with anti-FASTKD2 and anti-BrU antibodies. (C) Pixel colocalization image of BrU and FASTKD2 labelling in control fibroblasts. (D) Representative scatterplot of pixel intensity. X-axis: FASTKD2 signal. Y-axis: BrU signal. (E) Colocalization of FASTKD2 and BrU using Pearson's correlation coefficient and Manders' colocalization coefficient (M1 and M2).

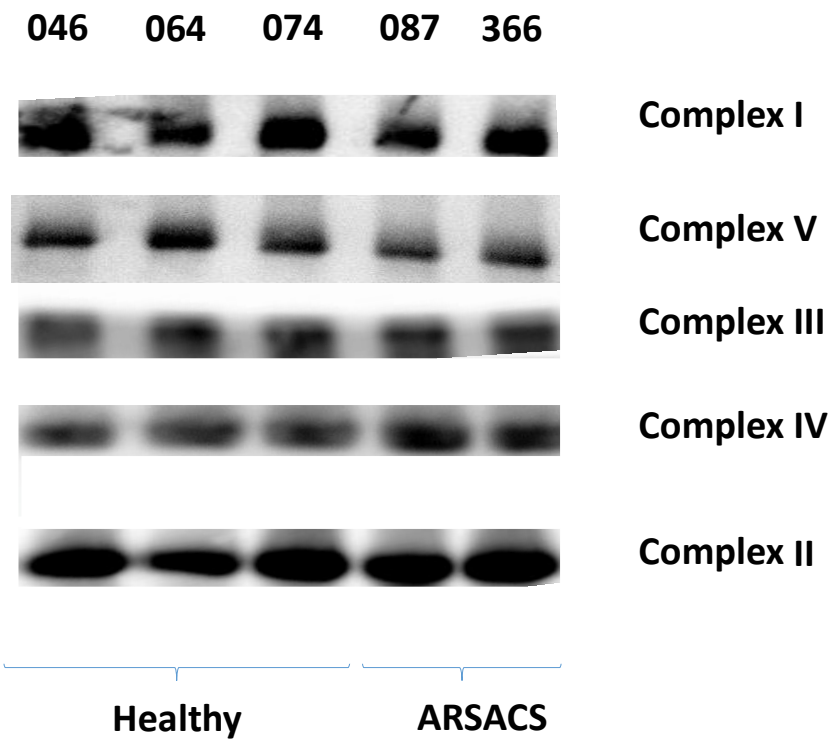

Figure 8: BN-PAGE analysis of the OXPHOS complexes in fibroblasts from control subjects (MCH046, MCH 064 and MCH074) and ARSACS patients (MCH087 and MCH366). Each of the five OXPHOS complexes (I–V) was visualized with a subunit specific antibody that recognizes the native complexes as follows: Complex I (NDUFA9), Complex II (SDHA), Complex III (UQCRC1), Complex IV (COX4), and Complex V (ATP5A1). Complex II is the loading control. ARSACS patient mitochondria show no apparent change in the total amount of fully assembled respiratory chain complexes.

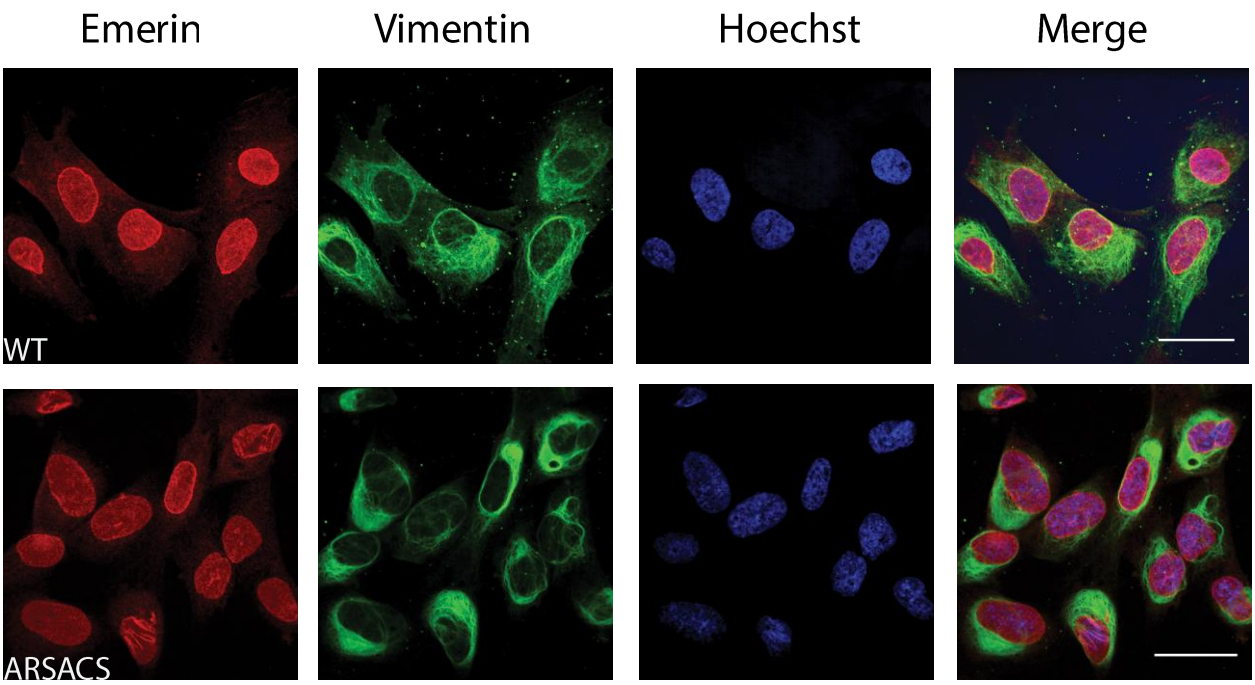

Figure 9: Emerin localization is normal in ARSACS fibroblasts despite presence of vimentin bundles. Double label of cultured fibroblasts with an antibodies against vimentin (green) and emerin (red). Nuclear DNA was additionally stained with Hoechst 33342. Scale bars denote 30 µm.

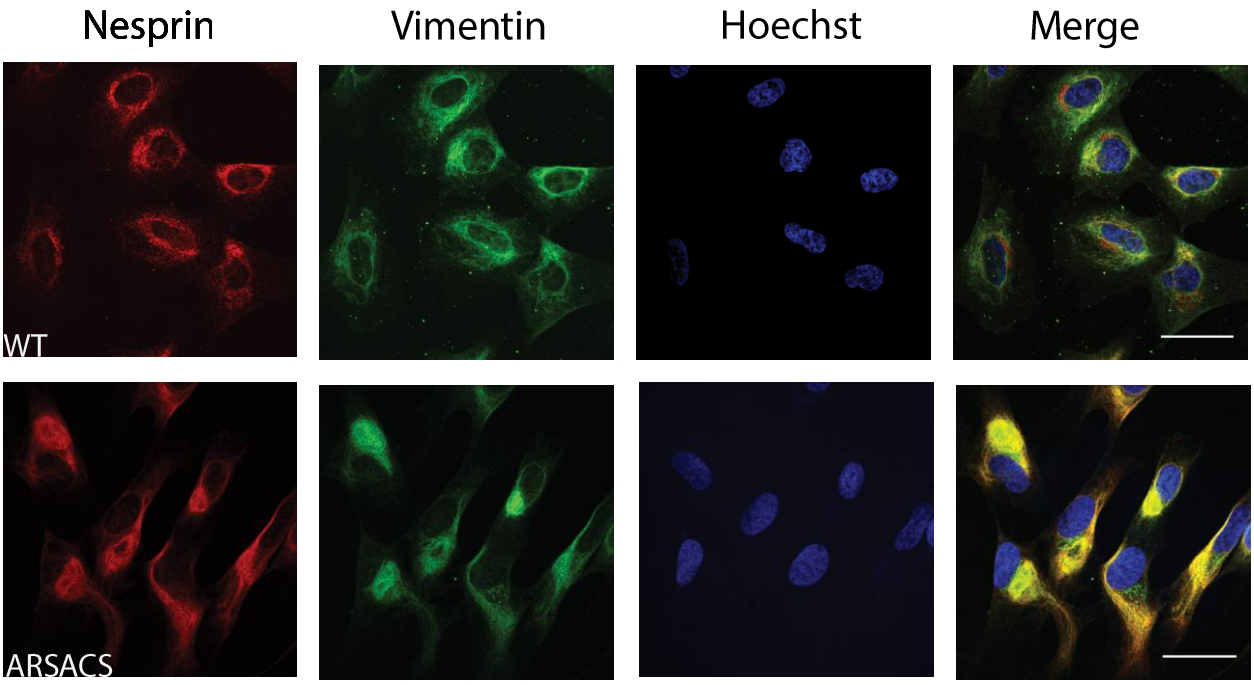

Figure 10: Nesprin3 mislocalizes to vimentin bundles in ARSACS fibroblasts. Double label of cultured fibroblasts with an antibodies against vimentin (green) and nesprin3 (red). Nuclear DNA was additionally stained with Hoechst 33342. Scale bars denote 30 µm.

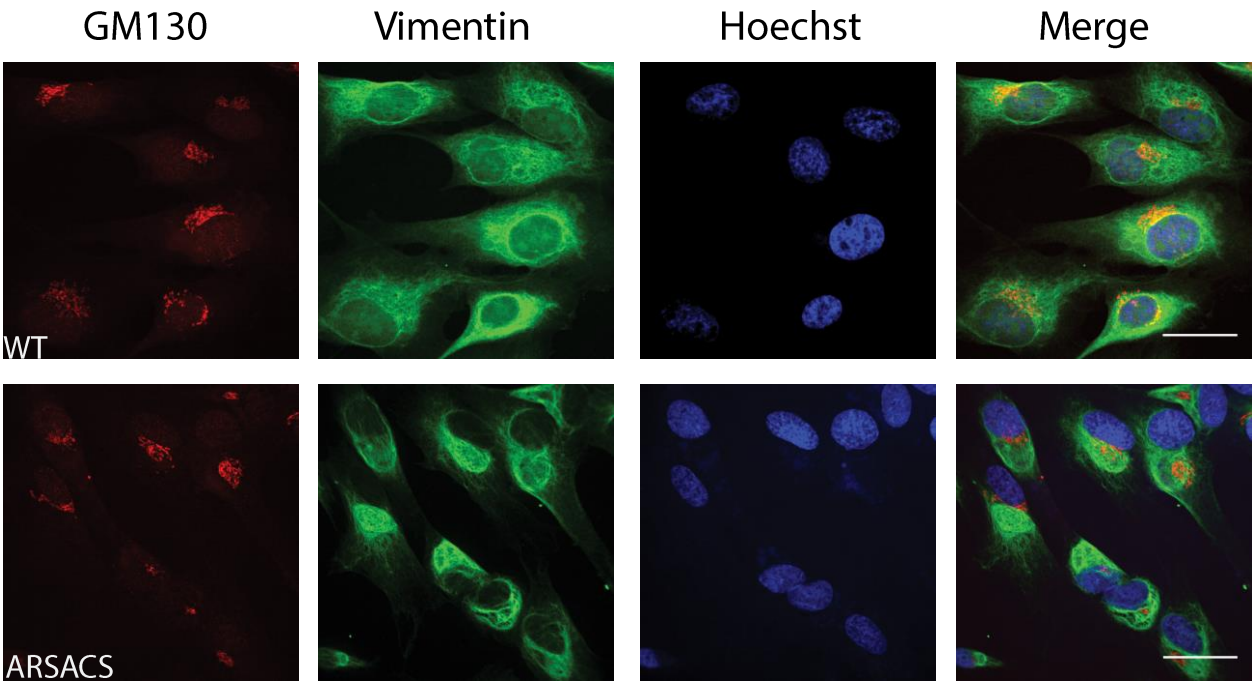

Figure 11: Distribution of the Golgi apparatus appears normal in ARSACS fibroblasts with vimentin bundling Double label of cultured fibroblasts with an antibodies against vimentin (green) and GM130 (red). Nuclear DNA was additionally stained with Hoechst 33342. Scale bars denote 30 µm.

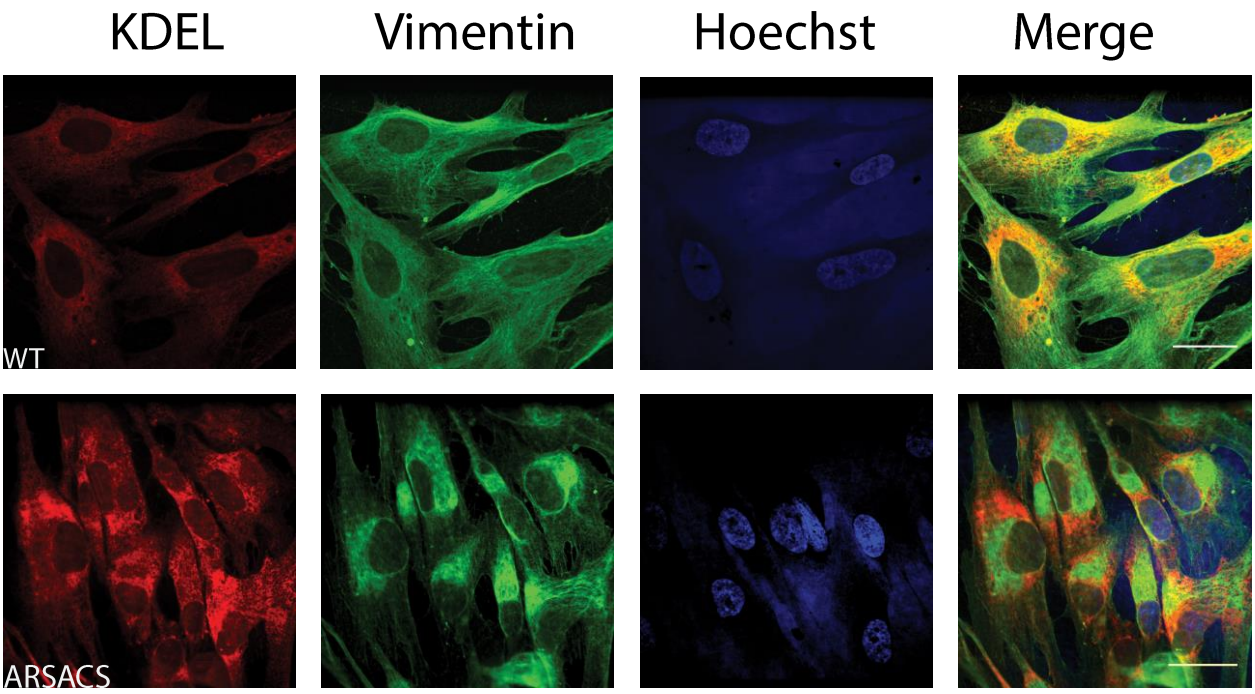

Figure 12: The endoplasmic reticulum is displaced by vimentin bundles in ARSACS fibroblasts. Double label of cultured fibroblasts with an antibodies against vimentin (green) and KDEL (red). Nuclear DNA was additionally stained with Hoechst 33342. Scale bars denote 30 µm.

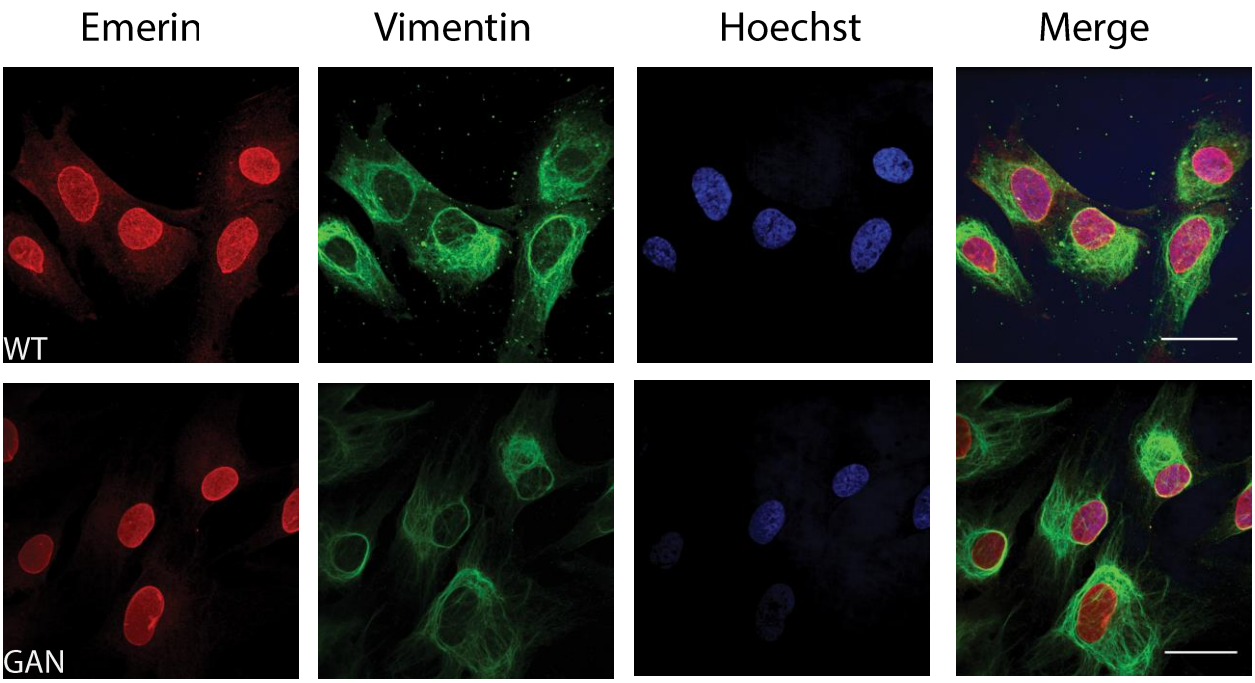

Figure 13. Emerin localization is normal in GAN fibroblasts despite presence of vimentin bundles. Double label of cultured fibroblasts with an antibodies against vimentin (green) and emerin (red). Nuclear DNA was additionally stained with Hoechst 33342. Scale bars denote 30 µm.

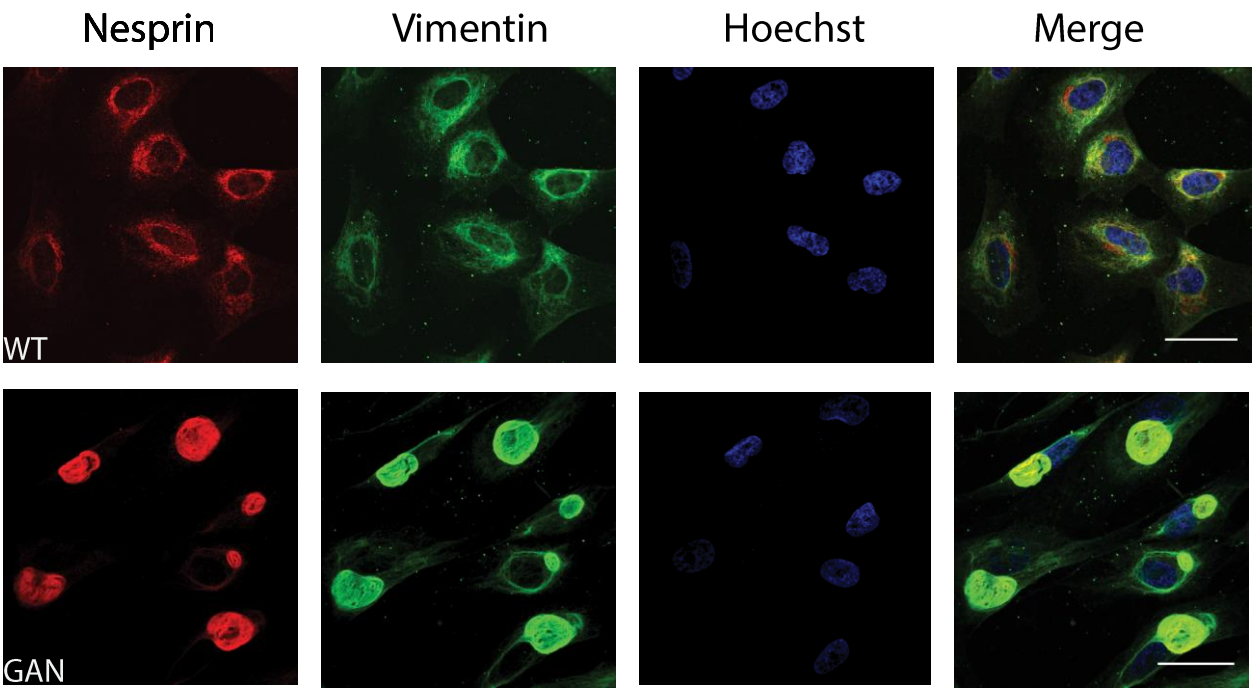

Figure 14: Nesprin3 mislocalizes to vimentin bundles in GAN fibroblasts. Double label of cultured fibroblasts with an antibodies against vimentin (green) and nesprin3 (red). Nuclear DNA was additionally stained with Hoechst 33342. Scale bars denote 30 µm.

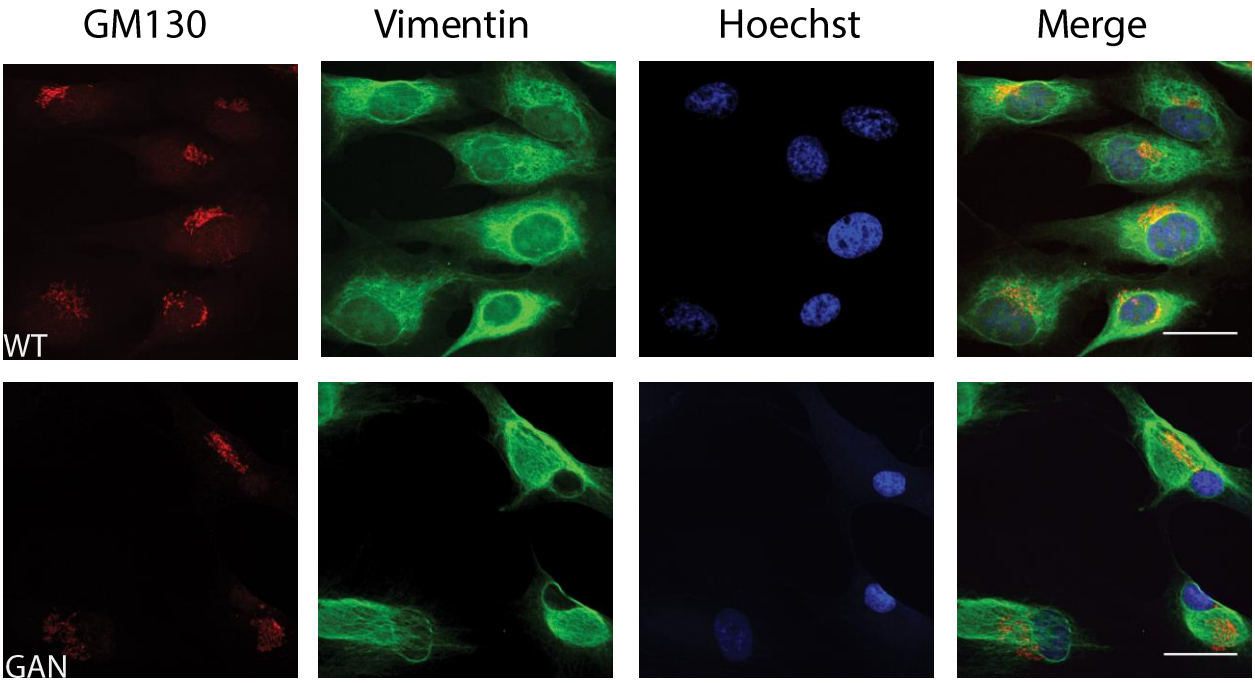

Figure 15: Distribution of the Golgi apparatus appears normal in GAN fibroblasts with vimentin bundling. Double label of cultured fibroblasts with an antibodies against vimentin (green) and GM130 (red). Nuclear DNA was additionally stained with Hoechst 33342. Scale bars denote 30 µm.

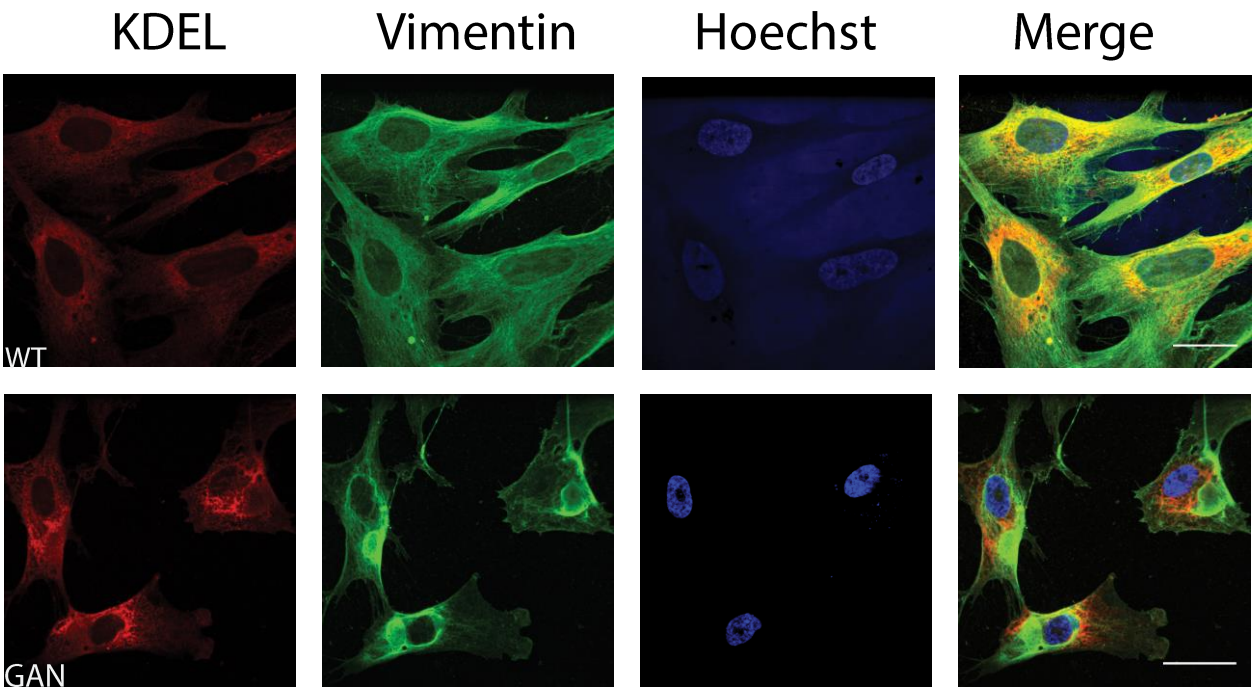

Figure 16: The endoplasmic reticulum is displaced by vimentin bundles in GAN fibroblasts. Double label of cultured fibroblasts with an antibodies against vimentin (green) and KDEL (red). Nuclear DNA was additionally stained with Hoechst 33342. Scale bars denote 30 µm.

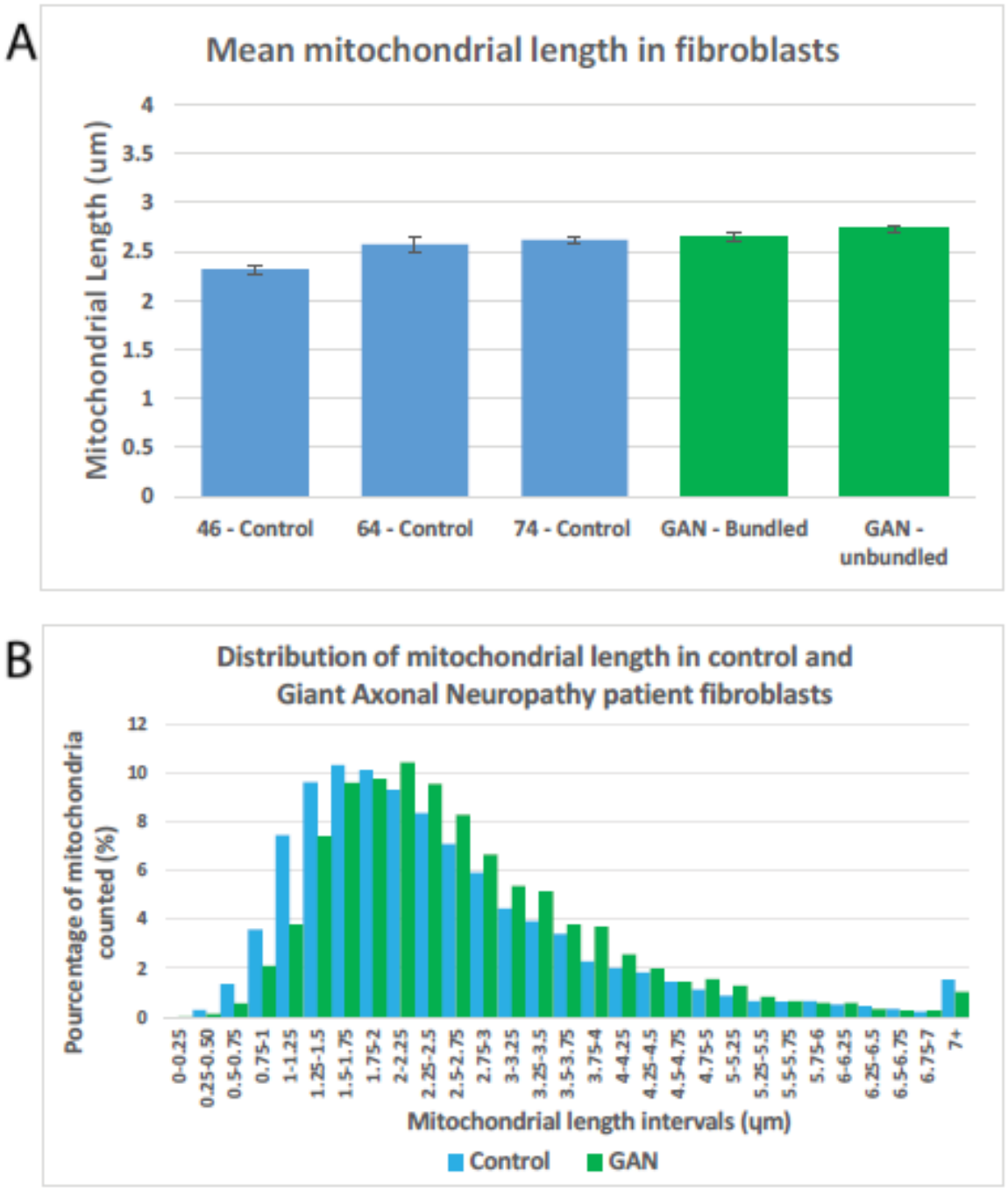
A
Mean mitochondrial length in fibroblasts
Mitochondrial Length (um)
4
3.5
3
2.5
2
1.5
1
0.5
0
46 - Control
64 - Control
74 - Control
GAN - Bundled
GAN - unbundled
B
Distribution of mitochondrial length in control and Giant Axonal Neuropathy patient fibroblasts
Pourcentage of mitochondria counted (%)
12
10
8
6
4
2
0
0-0.25
0.25-0.50
0.5-0.75
0.75-1
1-1.25
1.25-1.5
1.5-1.75
1.75-2
2-2.25
2.25-2.5
2.5-2.75
2.75-3
3-3.25
3.25-3.5
3.5-3.75
3.75-4
4-4.25
4.25-4.5
4.5-4.75
4.75-5
5-5.25
5.25-5.5
5.5-5.75
5.75-6
6-6.25
6.25-6.5
6.5-6.75
6.75-7
7+
Mitochondrial length intervals (µm)
Control
GAN

Figure 17.

Figure 17: Mitochondrial length distribution in cultured GAN patient fibroblasts are not longer than those in healthy control fibroblasts, regardless of the presence of vimentin aggregates. (A) Measurements of mean length of mitochondria in GAN patient fibroblasts (line WG791), categorized as BUNDLED or UNBUNDLED compared with control lines (MCH 046, MCG064 and MCH074). There was no significant difference ($p<0.05$; two-tailed t-test). (B) Comparison of distribution of mitochondrial lengths in cultured fibroblasts from a GAN patient (WG791) and healthy controls. Mitochondrial lengths have been binned into 0.25-μm intervals.

Chapter 5:

Discussion and conclusions

5.1. Mitochondrial length is significantly increased in dendrites of motor neurons in Sacs$^{-/-}$ mouse dissociated spinal cord-DRG cultures and in cultured ARSACS fibroblasts

The study reported in this thesis investigated if sacsin loss of function mutations are associated with mitochondrial dysfunction and linked to abnormalities in the intermediate filament network.

The size of sacsin protein and its number of domains make determining its function difficult and render ARSACS a complex disease to characterize, as it preferentially affects certain cell types and pathways. This study further characterized two cellular models: motor neurons in primary dissociated spinal cord-DR) cultures from *Sac* $^{-/-}$ mice and immortalized fibroblasts derived from patients' skin biopsies. Previous analysis of the motor neuron culture model showed good agreement with changes observed *in vivo* in the mouse model (Lariviere et al., 2014). Primary dissociated spinal cord-DRG cultures are time consuming to establish and yield a heterogeneous population of cells, making biochemical analysis of specific cell types unrealistic, but more closely representing a cell type involved in the human disease. Human fibroblasts are cultured quickly and provide a homogeneous culture that is more amenable to biochemical and morphological analysis due to its single cell type and planar configuration. To coordinate use of these two models experimentally, a comparison needed to be made between key ARSACS features found in primary culture and those found in fibroblasts.

The study first assessed mitochondrial length in primary dissociated spinal cord-DRG cultures of *Sacs*$^{-/-}$ mice. Motor neurons in the Sacs$^{-/-}$ cultures mature at a delayed rate, with the loss of peripherin expression characteristic of neuronal maturity occurring at five weeks of age instead of three weeks(Lariviere et al., 2014). Thus, cultures were evaluated at those two time

points. At both time points, there was a modest increase in mitochondrial length in motor neuron dendrites, with a corresponding shift in the distribution of mitochondrial lengths towards longer mitochondria. This significant difference in mean length matched the shift in length distribution. Of note were the population of very long mitochondria in ARSACS cells. At five weeks, there were relatively fewer mitochondria at the extremes of the distribution, indicating a possible compensatory effect. Previous measurements of mitochondrial length in axons in our group showed no increase in three-week-old cultures but a two-fold increase in axonal mitochondrial length at five weeks (Lariviere et al., 2014);however, the data are qualitatively similar. Mitochondrial length increases with time, and is not inherently abnormal when cultures are established.

Mitochondrial length is determined by the balance of fusion and fission. In the case of a sacsin loss of function mutation, decreased fission through loss of drp1 interaction could lead to longer mitochondria (Mils et al., 2015). Furthermore, if axonal mitochondria are a vulnerable subset of the mitochondrial population, they could be much more strongly affected by reduced mitochondrial fission. Dendritic mitochondria may more readily compensate to fission defects due to their proximity to the cell body, supporting the relatively modest increases in dendritic mitochondria length. Testing of this hypothesis would require measurement of mitochondrial fusion/fission in dendrites and axons in the same experiment.

A similar yet more pronounced increase in mitochondrial length was measured in human ARSACS patient fibroblasts, with an increase of roughly 30% when comparing pooled measurements from ARSACS and control lines. Additionally, the distribution of mitochondria was shifted towards longer mitochondria with an increased incidence of very long mitochondria

outside of the normal distribution. The increase in mitochondrial length is qualitatively similar in both motor neurons of *Sacs -/-* mice and patient fibroblasts.

5.2. No apparent defect in mitochondrial RNA transcription or RNA granule localization in Sacs$^{-/-}$ motor neurons or ARSACS fibroblasts

A possible cause of mitochondrial dysfunction is defects in synthesis of mitochondrial RNAs. Sacsin protein domains have potential roles in chaperone activity and DNA repair that could adversely affect localization or abundance of mitochondrial nucleic acids, thereby leading to downstream defects in RNA regulation or proper fission-fusion dynamics. Dysfunction of RNA granule formation or expression of RNA-binding proteins is characteristic of a number of mitochondrial diseases(Antonicka et al., 2013; Jourdain et al., 2013; Wolozin, 2012). RNA binding proteins are crucial for regulation of RNAs by dynamically controlling their localization, transport, translation, splicing and polyadenylation. An aspect of this posttranscriptional control involves consolidation of mitochondrial RNA into granules(Antonicka et al., 2013). These granules contain mRNAs that are translationally inert and respond to cellular stresses, regulate local mitochondrial translation or activate translational pathways during development(Antonicka et al., 2013).

In order to evaluate mtRNA synthesis and localization, incorporation of a labelled uridine analog, BrU, was used in tandem with immunolabeling of FASTKD2, a marker of RNA granules. Neither sacsin knockout in motor neurons nor loss of function mutation of sacsin in fibroblasts caused any significant change in incorporation of newly synthesized mitochondrial RNA into RNA granules, nor was there a change in RNA granule localization. This absence of

change indicated that these processes do not contribute to the increase in mitochondrial length, nor do these measures point to mitochondrial dysfunction in ARSACS.

In summary, there did not appear to be any defects in mtRNA incorporation and RNA granule localization in ARSACS fibroblasts.

5.3. No significant depletion of respiratory chain complexes in ARSACS fibroblasts

Mitochondria are critical in cellular energy generation. The ATP-generating structure in eukaryotic cells is the electron transport chain, the site of oxidative phosphorylation reactions comprised of five large multi-unit complexes (I, II, III, IV and V). During cellular respiration, an electrochemical gradient is generated by a series of redox reactions, which is coupled to the shuttling of protons out of the mitochondrial inner membrane. The proton gradient generated by electron transport allows protons to re-enter the mitochondrial inner membrane via the ATP synthase enzyme, thereby generating the cell's energetic currency.

A significant cause of mitochondrial dysfunction is a defect in the assembly of respiratory chain complexes. Deficiencies in complex assembly are linked to early-onset, severe disorders leading to a wide array ailments, such as neurological problems, seizures, diabetes, muscle weakness, developmental delays, among others (Distelmaier et al., 2009). Assessment of abundance of respiratory chain complexes using Blue Native PAGE showed no change when comparing healthy control fibroblasts with those of ARSACS patients. However, mitochondrial fractions were compared and thus, this experiment did not control for the abundance of mitochondria within individual cells. While there is no difference in relative abundance of oxidative phosphorylation complexes, it does not preclude a deficiency in mitochondrial mass

per cell. This could be assessed by measuring cellular respiration by oxygraphy using a clark-type electrode.

The comparison between cellular models highlights both strengths and weaknesses for future ARSACS research with regards to mitochondria. Primary cultured *Sacs*$^{-/-}$ mouse motor neurons demonstrate a mitochondrial length phenotype that can be tracked over time. This model revealed that the mitochondrial phenotype developed over time, and was not inherent when the spinal cord-DRG cultures were established. Rather it is a relatively late phenomenon commensurate with obvious neurofilament bundling (Lariviere et al., 2014).

5.4. Effect of altered intermediate filament organization on distribution of the Golgi, endoplasmic reticulum (ER) and nucleus in ARSACS cells.

In other neurodegenerative diseases, deformations in organelles are a common secondary effect of intermediate filament dysfunction. To determine how changes in intermediate filament organization affect key organelles, immunocytochemistry was performed using antibodies against the Golgi apparatus, endoplasmic reticulum, proteins associated with the nucleus and LINC assembly regulating nuclear placement (emerin and nesprin3).

Localization of the Golgi apparatus did not appear to be abnormal in ARSACS patient fibroblasts. With regards to the endoplasmic reticulum, vimentin aggregates were sufficiently dense to force deformation of the ER around the bundles. Intermediate filaments can interact with ER, but in this case, the redistribution of ER seemed passive.

Examining the LINC complex, nesprin3 closely colocalized with vimentin bundles in ARSACS patient fibroblasts while emerin maintained perinuclear localization identical to

controls. The vimentin aggregation seen in ARSACS fibroblasts appears to impair the link between nesprin-3 and emerin.

5.5. The intermediate filament disorganization in ARSACS is similar to GAN, but the elongation of mitochondria is unique to ARSACS).

It remained unknown whether the mitochondrial phenotype or the effects on LINC complex regulation of nuclear positioning present in ARSACS was a consequence of the bundling and collapse of the intermediate filament network or an independent effect of loss of sacsin function. Therefore, comparison of the intermediate filament and mitochondrial phenotype present in ARSACS fibroblasts prompted investigation into human fibroblasts from patients with Giant Axonal Neuropathy (GAN), a neurological disease with a primary intermediate filament pathology. A percentage of GAN fibroblasts display prominent spherical vimentin aggregates, even more prominent than the bundles seen in ARSACS fibroblasts. Nevertheless, the effect of these bundles on organelle and nuclear scaffolding proteins mirrors that of ARSACS: The Golgi apparatus and emerin are both unchanged compared to control fibroblasts, however ER localization is displaced by vimentin bundles. Nesprin3 has a similar phenotype as ARSACS fibroblasts in that it extensively colocalizes with vimentin aggregates and has a largely decreased perinuclear component.

However, despite the similarities in intermediate filament, organelle and scaffold phenotypes, the mitochondrial length increase characteristic of ARSACS was not recapitulated in GAN fibroblasts, independent of vimentin aggregation state. Whether or not vimentin forms bundles in GAN fibroblasts, there was no significant change in mitochondrial length, nor was

there a shift in distribution of mitochondrial length distribution. Current knowledge on ARSACS places significant importance of mitochondria as the primary agent for the neuropathology of the disease. However, through comparison of cytoskeletal organization and mitochondrial length in another model of neurodegeneration (GAN) there is a notable separation between the two. It appears that while cytoskeletal organization and mitochondrial length may linked, the intermediate filament phenotype itself does not appear to be responsible for mitochondrial changes in ARSACS.

5.6. Contributions of the study

5.6.1. Experimental model development

The use of both primary cultured *Sac* $^{-/-}$ mouse motor neurons and cultured ARSACS patient fibroblasts in this study served to develop experimental models of disease by providing direct comparison of the mitochondrial and intermediate filament phenotypes that arise. Both IF bundling and mitochondrial length increases occur in both models, However, while primary motor neurons demonstrate a similar overall phenotype to ARSACS patients, fibroblasts are more amenable to biochemical assays to more thoroughly dissect elements of morphological change and prove advantageous in adequately recapitulating molecular events that occur in motor neurons in ARSACS patients. This study suggests that use of fibroblasts as an initial model for preliminary biochemical and morphological experiments is appropriate due to the uniform cell-type and experimental versatility provided by such a culture. The primary mouse motor neuron culture is a more rigorous experimental model that more closely models ARSACS

patient cells and should be used to confirm and further elaborate promising preliminary results. However, it presents pitfalls such as the difficulties noted in studying BrU incorporation and the impossibility of certain biochemical assays such as BN-PAGE.

Why are mitochondria affected in ARSACS and appear unaffected in the line of GAN fibroblasts that were investigated? Why are there ER and nesprin-3 displaced in both GAN and ARSACS, yet emerin and the Golgi apparatus remain unaffected? Direct comparison of sacsin and gigaxonin is difficult, given the size of sacsin and poorly characterized nature of both proteins. However, some inferences can be made as to the causes of each phenotype demonstrated. Importantly, the core similarity between gigaxonin and sacsin dysfunction lies in the disorganization of the intermediate filament network. Intermediate filaments are known to interact with the ER and with the outer nuclear membrane (and thus nesprin-3) and disruption of the intermediate filament network is more likely to affect their organization (Ketema, Kreft, Secades, Janssen, & Sonnenberg, 2013). Plus, the perinuclear vimentin inclusions physically exclude other organelles. However, organelles that are have fewer direct contacts with intermediate filaments, such as the Golgi apparatus, are likely to be less affected by their bundling. Finally emerin, as a protein located *within* the inner nuclear envelope is neither displaced by vimentin deformation nor disrupted because of interactions with vimentin. Mitochondria may only be affected in ARSACS because gigaxonin does not share sacsin's interaction with mitochondrial fission/fusion machinery through Drp1 (Girard et al., 2012). Disruption of this machinery could account for the different mitochondrial properties seen in human fibroblasts derived from each disease.

5.6.2. Mitochondrial dysfunction is not a direct result of intermediate filament network collapse as it does not occur in GAN

This study demonstrated modest increases in mitochondrial length in *Sac* $^{-/-}$ mouse motor neuron dendrites at three weeks in culture that persist through neuronal maturation. This increase is qualitatively the same as seen in motor neuron axons. Furthermore, in both primary *Sacs*$^{-/-}$ mouse motor neurons and immortalized fibroblasts derived from ARSACS patient skin biopsies, intermediate filament organization was disrupted in a manner that caused deformation of organelles such as the endoplasmic reticulum and the outer nuclear membrane component of the LINC complex. It established that binding between the protein structures responsible for anchoring the nucleus to the cytoskeleton was disrupted through vimentin bundling and mislocalization of nesprin3, demonstrating disorganization at the level of the nuclear outer membrane.

The study of GAN fibroblasts demonstrated that alteration in mitochondrial length and distribution seen in ARSACS is not a typical secondary consequence of the collapse of the intermediate filament network. Sacsin could have regulatory effects on multiple proteins that act on both mitochondrial dynamics and intermediate filament distribution, although they appear to be independent consequences of the sacsin mutation.

Both the DnaJ and UbL domains of sacsin might play roles in proteostasis by clearing misfolded proteins and by regulating transcription through interactions with transcription factors. This is accomplished mainly through interaction with the UPS and Hsp40 and Hsp70 activity. In addition, the XPCB domain of sacsin has been associated with both the UPS pathway and nucleotide excision repair. While loss of function of these domains may not have caused an

apparent defect in mtRNA transcription or assembly of oxidative phosphorylation complexes, defects in chaperone activity or effective protein turnover could have other effects regulating mitochondrial dynamics that affect function. Additionally, similar mechanisms involving different proteins could disrupt organization of the cytoskeletal network. For example, gigaxonin, the protein whose loss is responsible for GAN, interacts with ubiquitin-like modifier activating enzyme 1 (UBE1). This protein acts on the NEDD8 pathway and is a catalyst for the adenylation of ubiquitin. This targets proteins for degradation by the proteasome. Furthermore, UBE1 mutation has been linked to spinal muscular atrophy, another neurodegenerative disease. It is plausible that loss of sacsin may cause defects in proteasome or chaperone activity that could be related to both intermediate filament proteins and proteins that regulate mitochondrial morphology.

References

Al-Chalabi, A., & Miller, C. C. (2003). Neurofilaments and neurological disease. *Bioessays, 25*(4), 346-355. doi: 10.1002/bies.10251

Anderson, J. F., Siller, E., & Barral, J. M. (2010). The sacsin repeating region (SRR): a novel Hsp90-related supra-domain associated with neurodegeneration. *J Mol Biol, 400*(4), 665-674. doi: 10.1016/j.jmb.2010.05.023

Anderson, J. F., Siller, E., & Barral, J. M. (2011). The neurodegenerative-disease-related protein sacsin is a molecular chaperone. *J Mol Biol, 411*(4), 870-880. doi: 10.1016/j.jmb.2011.06.016

Anderson, S., Bankier, A. T., Barrell, B. G., de Bruijn, M. H., Coulson, A. R., Drouin, J., . . . Young, I. G. (1981). Sequence and organization of the human mitochondrial genome. *Nature, 290*(5806), 457-465.

Anheim, M. (2011). Autosomal recessive cerebellar ataxias. *Revue neurologique, 167*(5), 372-384. doi: 10.1016/j.neurol.2010.07.021 [doi]

Antonicka, H., Sasarman, F., Nishimura, T., Paupe, V., & Shoubridge, E. A. (2013). The mitochondrial RNA-binding protein GRSF1 localizes to RNA granules and is required for posttranscriptional mitochondrial gene expression. *Cell metabolism, 17*(3), 386-398. doi: 10.1016/j.cmet.2013.02.006 [doi]

Baas, P. W., & Black, M. M. (1990). Individual microtubules in the axon consist of domains that differ in both composition and stability. *J Cell Biol, 111*(2), 495-509.

Barry, D. M., Millecamps, S., Julien, J. P., & Garcia, M. L. (2007). New movements in neurofilament transport, turnover and disease. *Exp Cell Res, 313*(10), 2110-2120. doi: 10.1016/j.yexcr.2007.03.011

Bearer, E. L., & Reese, T. S. (1999). Association of actin filaments with axonal microtubule tracts. *J Neurocytol, 28*(2), 85-98.

Beaulieu, J. M., Kriz, J., & Julien, J. P. (2002). Induction of peripherin expression in subsets of brain neurons after lesion injury or cerebral ischemia. *Brain Res, 946*(2), 153-161.

Bouchard, J. P., Barbeau, A., Bouchard, R., & Bouchard, R. W. (1978). Autosomal recessive spastic ataxia of Charlevoix-Saguenay. *Can J Neurol Sci, 5*(1), 61-69.

Bouchard, J. P., Richter, A., Mathieu, J., Brunet, D., Hudson, T. J., Morgan, K., & Melancon, S. B. (1998). Autosomal recessive spastic ataxia of Charlevoix-Saguenay. *Neuromuscul Disord, 8*(7), 474-479.

Bouhlal, Y., Amouri, R., El Euch-Fayeche, G., & Hentati, F. (2011). Autosomal recessive spastic ataxia of Charlevoix-Saguenay: an overview. *Parkinsonism & related disorders, 17*(6), 418-422. doi: 10.1016/j.parkreldis.2011.03.005 [doi]

Brown, A. (1997). Visualization of single neurofilaments by immunofluorescence microscopy of splayed axonal cytoskeletons. *Cell Motil Cytoskeleton, 38*(2), 133-145. doi: 10.1002/(sici)1097-0169(1997)38:2<133::aid-cm3>3.0.co;2-8

Brown, H. G., Troncoso, J. C., & Hoh, J. H. (1998). Neurofilament-L homopolymers are less mechanically stable than native neurofilaments. *J Microsc, 191*(3), 229-237.

Brownlees, J., Ackerley, S., Grierson, A. J., Jacobsen, N. J., Shea, K., Anderton, B. H., . . . Miller, C. C. (2002). Charcot-Marie-Tooth disease neurofilament mutations disrupt neurofilament assembly and axonal transport. *Hum Mol Genet, 11*(23), 2837-2844.

Busch, K. B., Kowald, A., & Spelbrink, J. N. (2014a). Quality matters: how does mitochondrial network dynamics and quality control impact on mtDNA integrity? *Philos Trans R Soc Lond B Biol Sci, 369*(1646), 20130442. doi: 10.1098/rstb.2013.0442

Busch, K. B., Kowald, A., & Spelbrink, J. N. (2014b). Quality matters: how does mitochondrial network dynamics and quality control impact on mtDNA integrity? *Philosophical transactions of the Royal Society of London.Series B, Biological sciences, 369*(1646), 20130442. doi: 10.1098/rstb.2013.0442 [doi]

Capetanaki, Y., Milner, D. J., & Weitzer, G. (1997). Desmin in muscle formation and maintenance: knockouts and consequences. *Cell Struct Funct, 22*(1), 103-116.

Chaban, Y., Boekema, E. J., & Dudkina, N. V. (2014). Structures of mitochondrial oxidative phosphorylation supercomplexes and mechanisms for their stabilisation. *Biochim Biophys Acta, 1837*(4), 418-426. doi: 10.1016/j.bbabio.2013.10.004

Chen, H., & Chan, D. C. (2009). Mitochondrial dynamics--fusion, fission, movement, and mitophagy--in neurodegenerative diseases. *Hum Mol Genet, 18*(R2), R169-176. doi: 10.1093/hmg/ddp326

Cochard, P., & Paulin, D. (1984). Initial expression of neurofilaments and vimentin in the central and peripheral nervous system of the mouse embryo in vivo. *J Neurosci, 4*(8), 2080-2094.

Collard, J. F., Cote, F., & Julien, J. P. (1995). Defective axonal transport in a transgenic mouse model of amyotrophic lateral sclerosis. *Nature, 375*(6526), 61-64. doi: 10.1038/375061a0

Conde, C., & Caceres, A. (2009). Microtubule assembly, organization and dynamics in axons and dendrites. *Nat Rev Neurosci, 10*(5), 319-332. doi: 10.1038/nrn2631

De Braekeleer, M., Giasson, F., Mathieu, J., Roy, M., Bouchard, J. P., & Morgan, K. (1993). Genetic epidemiology of autosomal recessive spastic ataxia of Charlevoix-Saguenay in northeastern Quebec. *Genet Epidemiol, 10*(1), 17-25. doi: 10.1002/gepi.1370100103

de Brito, O. M., & Scorrano, L. (2010). An intimate liaison: spatial organization of the endoplasmic reticulum-mitochondria relationship. *Embo j, 29*(16), 2715-2723. doi: 10.1038/emboj.2010.177

Detmer, S. A., & Chan, D. C. (2007). Functions and dysfunctions of mitochondrial dynamics. *Nat Rev Mol Cell Biol, 8*(11), 870-879. doi: 10.1038/nrm2275

Distelmaier, F., Koopman, W. J., van den Heuvel, L. P., Rodenburg, R. J., Mayatepek, E., Willems, P. H., & Smeitink, J. A. (2009). Mitochondrial complex I deficiency: from organelle dysfunction to clinical disease. *Brain, 132*(Pt 4), 833-842. doi: 10.1093/brain/awp058

Duchen, M. R., & Szabadkai, G. (2010). Roles of mitochondria in human disease. *Essays Biochem, 47*, 115-137. doi: 10.1042/bse0470115

Ehlers, M. D., Fung, E. T., O'Brien, R. J., & Huganir, R. L. (1998). Splice variant-specific interaction of the NMDA receptor subunit NR1 with neuronal intermediate filaments. *J Neurosci, 18*(2), 720-730.

Engert, J. C., Berube, P., Mercier, J., Dore, C., Lepage, P., Ge, B., . . . Richter, A. (2000). ARSACS, a spastic ataxia common in northeastern Quebec, is caused by mutations in a new gene encoding an 11.5-kb ORF. *Nat Genet, 24*(2), 120-125. doi: 10.1038/72769

Fifkova, E., & Delay, R. J. (1982). Cytoplasmic actin in neuronal processes as a possible mediator of synaptic plasticity. *J Cell Biol, 95*(1), 345-350.

Fogel, B. L., & Perlman, S. (2007). Clinical features and molecular genetics of autosomal recessive cerebellar ataxias. *Lancet Neurol, 6*(3), 245-257. doi: 10.1016/s1474-4422(07)70054-6

Foisner, R., Leichtfried, F. E., Herrmann, H., Small, J. V., Lawson, D., & Wiche, G. (1988). Cytoskeleton-associated plectin: in situ localization, in vitro reconstitution, and binding to immobilized intermediate filament proteins. *J Cell Biol, 106*(3), 723-733.

Friedland-Leuner, K., Stockburger, C., Denzer, I., Eckert, G. P., & Muller, W. E. (2014). Mitochondrial dysfunction: cause and consequence of Alzheimer's disease. *Prog Mol Biol Transl Sci, 127*, 183-210. doi: 10.1016/b978-0-12-394625-6.00007-6

Gagnon, C., Lavoie, C., Lessard, I., Mathieu, J., Brais, B., Bouchard, J. P., . . . Lambercy, O. (2014). The Virtual Peg Insertion Test as an assessment of upper limb coordination in ARSACS patients: a pilot study. *J Neurol Sci, 347*(1-2), 341-344. doi: 10.1016/j.jns.2014.09.032

Ganay, T., Boizot, A., Burrer, R., Chauvin, J. P., & Bomont, P. (2011). Sensory-motor deficits and neurofilament disorganization in gigaxonin-null mice. *Mol Neurodegener, 6*, 25. doi: 10.1186/1750-1326-6-25

Gao, Y., & Sztul, E. (2001). A novel interaction of the Golgi complex with the vimentin intermediate filament cytoskeleton. *J Cell Biol, 152*(5), 877-894.

Garcia-Martin, E., Pablo, L. E., Gazulla, J., Polo, V., Ferreras, A., & Larrosa, J. M. (2013). Retinal nerve fibre layer thickness in ARSACS: myelination or hypertrophy? *Br J Ophthalmol, 97*(2), 238-241. doi: 10.1136/bjophthalmol-2012-302309 [doi]

Gentil, B. J., & Cooper, L. (2012). Molecular basis of axonal dysfunction and traffic impairments in CMT. *Brain Res Bull, 88*(5), 444-453. doi: 10.1016/j.brainresbull.2012.05.003

Gentil, B. J., Minotti, S., Beange, M., Baloh, R. H., Julien, J. P., & Durham, H. D. (2012). Normal role of the low-molecular-weight neurofilament protein in mitochondrial dynamics and disruption in Charcot-Marie-Tooth disease. *Faseb j, 26*(3), 1194-1203. doi: 10.1096/fj.11-196345

Gentil, B. J., Tibshirani, M., & Durham, H. D. (2015). Neurofilament dynamics and involvement in neurological disorders. *Cell Tissue Res, 360*(3), 609-620. doi: 10.1007/s00441-014-2082-7

Girard, M., Lariviere, R., Parfitt, D. A., Deane, E. C., Gaudet, R., Nossova, N., . . . McPherson, P. S. (2012). Mitochondrial dysfunction and Purkinje cell loss in autosomal recessive spastic ataxia of Charlevoix-Saguenay (ARSACS). *Proc Natl Acad Sci U S A, 109*(5), 1661-1666. doi: 10.1073/pnas.1113166109 [doi]

Gomez, C. M. (2004). ARSACS goes global. *Neurology, 62*(1), 10-11.

Grenier, K., McLelland, G. L., & Fon, E. A. (2013). Parkin- and PINK1-Dependent Mitophagy in Neurons: Will the Real Pathway Please Stand Up? *Front Neurol, 4*, 100. doi: 10.3389/fneur.2013.00100

Grieco, G. S., Malandrini, A., Comanducci, G., Leuzzi, V., Valoppi, M., Tessa, A., . . . Santorelli, F. M. (2004). Novel SACS mutations in autosomal recessive spastic ataxia of Charlevoix-Saguenay type. *Neurology, 62*(1), 103-106.

Grynberg, M., Erlandsen, H., & Godzik, A. (2003). HEPN: a common domain in bacterial drug resistance and human neurodegenerative proteins. *Trends Biochem Sci, 28*(5), 224-226. doi: 10.1016/s0968-0004(03)00060-4

Hroudova, J., & Singh, N. (2014). Mitochondrial dysfunctions in neurodegenerative diseases: relevance to Alzheimer's disease. *2014*, 175062. doi: 10.1155/2014/175062

Jourdain, A. A., Koppen, M., Wydro, M., Rodley, C. D., Lightowlers, R. N., Chrzanowska-Lightowlers, Z. M., & Martinou, J. C. (2013). GRSF1 regulates RNA processing in mitochondrial RNA granules. *Cell metabolism, 17*(3), 399-410. doi: 10.1016/j.cmet.2013.02.005 [doi]

Julien, J. P. (1997). Neurofilaments and motor neuron disease. *Trends Cell Biol, 7*(6), 243-249. doi: 10.1016/s0962-8924(97)01049-0

Kamada, S., Okawa, S., Imota, T., Sugawara, M., & Toyoshima, I. (2008). Autosomal recessive spastic ataxia of Charlevoix-Saguenay (ARSACS): novel compound heterozygous mutations in the SACS gene. *J Neurol, 255*(6), 803-806. doi: 10.1007/s00415-008-0672-6

Kamionka, M., & Feigon, J. (2004). Structure of the XPC binding domain of hHR23A reveals hydrophobic patches for protein interaction. *Protein Sci, 13*(9), 2370-2377. doi: 10.1110/ps.04824304

Karpova, A., Mikhaylova, M., Bera, S., Bar, J., Reddy, P. P., Behnisch, T., . . . Kreutz, M. R. (2013). Encoding and transducing the synaptic or extrasynaptic origin of NMDA receptor signals to the nucleus. *Cell, 152*(5), 1119-1133. doi: 10.1016/j.cell.2013.02.002

Ketema, M., Kreft, M., Secades, P., Janssen, H., & Sonnenberg, A. (2013). Nesprin-3 connects plectin and vimentin to the nuclear envelope of Sertoli cells but is not required for Sertoli cell function in spermatogenesis. *Mol Biol Cell, 24*(15), 2454-2466. doi: 10.1091/mbc.E13-02-0100

Kowald, A., & Kirkwood, T. B. (2011). Evolution of the mitochondrial fusion-fission cycle and its role in aging. *Proc Natl Acad Sci U S A, 108*(25), 10237-10242. doi: 10.1073/pnas.1101604108

Kozlov, G., Denisov, A. Y., Girard, M., Dicaire, M. J., Hamlin, J., McPherson, P. S., . . . Gehring, K. (2011). Structural basis of defects in the sacsin HEPN domain responsible for autosomal recessive spastic ataxia of Charlevoix-Saguenay (ARSACS). *The Journal of biological chemistry, 286*(23), 20407-20412. doi: 10.1074/jbc.M111.232884 [doi]

Lariviere, R., Gaudet, R., Gentil, B. J., Girard, M., Conte, T. C., Minotti, S., . . . Brais, B. (2014). Sacs knockout mice present pathophysiological defects underlying autosomal recessive spastic ataxia of Charlevoix-Saguenay. *Hum Mol Genet*. doi: 10.1093/hmg/ddu491

Legros, F., Lombes, A., Frachon, P., & Rojo, M. (2002). Mitochondrial fusion in human cells is efficient, requires the inner membrane potential, and is mediated by mitofusins. *Mol Biol Cell, 13*(12), 4343-4354. doi: 10.1091/mbc.E02-06-0330

Macioce, P., Gandolfi, N., Leung, C. L., Chin, S. S., Malchiodi-Albedi, F., Ceccarini, M., . . . Liem, R. K. (1999). Characterization of NF-L and betaIISigma1-spectrin interaction in live cells. *Exp Cell Res, 250*(1), 142-154. doi: 10.1006/excr.1999.4479

Martikainen, M. H., & Chinnery, P. F. (2015). Mitochondrial disease: mimics and chameleons. *Pract Neurol*. doi: 10.1136/practneurol-2015-001191

Miller, C. C., Ackerley, S., Brownlees, J., Grierson, A. J., Jacobsen, N. J., & Thornhill, P. (2002). Axonal transport of neurofilaments in normal and disease states. *Cell Mol Life Sci, 59*(2), 323-330.

Mils, V., Bosch, S., Roy, J., Bel-Vialar, S., Belenguer, P., Pituello, F., & Miquel, M. C. (2015). Mitochondrial reshaping accompanies neural differentiation in the developing spinal cord. *PLoS One, 10*(5), e0128130. doi: 10.1371/journal.pone.0128130

Miyata, M., Kishimoto, Y., Tanaka, M., Hashimoto, K., Hirashima, N., Murata, Y., . . . Takagishi, Y. (2011). A role for myosin Va in cerebellar plasticity and motor learning: a possible mechanism underlying neurological disorder in myosin Va disease. *J Neurosci, 31*(16), 6067-6078. doi: 10.1523/jneurosci.5651-10.2011

Miyatake, S., Miyake, N., Doi, H., Saitsu, H., Ogata, K., Kawai, M., & Matsumoto, N. (2012). A novel SACS mutation in an atypical case with autosomal recessive spastic ataxia of Charlevoix-Saguenay (ARSACS). *Intern Med, 51*(16), 2221-2226.

Morgan, J. T., Pfeiffer, E. R., Thirkill, T. L., Kumar, P., Peng, G., Fridolfsson, H. N., . . . Barakat, A. I. (2011). Nesprin-3 regulates endothelial cell morphology, perinuclear cytoskeletal architecture, and flow-induced polarization. *Mol Biol Cell, 22*(22), 4324-4334. doi: 10.1091/mbc.E11-04-0287

Mrissa, N., Belal, S., Hamida, C. B., Amouri, R., Turki, I., Mrissa, R., . . . Hentati, F. (2000). Linkage to chromosome 13q11-12 of an autosomal recessive cerebellar ataxia in a Tunisian family. *Neurology, 54*(7), 1408-1414.

Ogawa, T., Takiyama, Y., Sakoe, K., Mori, K., Namekawa, M., Shimazaki, H., . . . Nishizawa, M. (2004). Identification of a SACS gene missense mutation in ARSACS. *Neurology, 62*(1), 107-109.

Ouyang, Y., Segers, K., Bouquiaux, O., Wang, F. C., Janin, N., Andris, C., . . . Takiyama, Y. (2008). Novel SACS mutation in a Belgian family with sacsin-related ataxia. *J Neurol Sci, 264*(1-2), 73-76. doi: 10.1016/j.jns.2007.07.022

Pablo, L. E., Garcia-Martin, E., Gazulla, J., Larrosa, J. M., Ferreras, A., Santorelli, F. M., . . . Marin, M. A. (2011). Retinal nerve fiber hypertrophy in ataxia of Charlevoix-Saguenay patients. *Molecular vision, 17*, 1871-1876. doi: 204 [pii]

Parfitt, D. A., Michael, G. J., Vermeulen, E. G., Prodromou, N. V., Webb, T. R., Gallo, J. M., . . . Chapple, J. P. (2009). The ataxia protein sacsin is a functional co-chaperone that protects against polyglutamine-expanded ataxin-1. *Hum Mol Genet, 18*(9), 1556-1565. doi: 10.1093/hmg/ddp067

Pedroso, J. L., Braga-Neto, P., Abrahao, A., Rivero, R. L., Abdalla, C., Abdala, N., & Barsottini, O. G. (2011). Autosomal recessive spastic ataxia of Charlevoix-Saguenay (ARSACS): typical clinical and neuroimaging features in a Brazilian family. *Arquivos de Neuro-Psiquiatria, 69*(2B), 288-291. doi: S0004-282X2011000300004 [pii]

Pena, S. D. (1982). Giant axonal neuropathy: an inborn error of organization of intermediate filaments. *Muscle Nerve, 5*(2), 166-172. doi: 10.1002/mus.880050215

Rao, M. V., Engle, L. J., Mohan, P. S., Yuan, A., Qiu, D., Cataldo, A., . . . Nixon, R. A. (2002). Myosin Va binding to neurofilaments is essential for correct myosin Va distribution and transport and neurofilament density. *J Cell Biol, 159*(2), 279-290. doi: 10.1083/jcb.200205062

Rao, M. V., Mohan, P. S., Kumar, A., Yuan, A., Montagna, L., Campbell, J., . . . Nixon, R. A. (2011). The myosin Va head domain binds to the neurofilament-L rod and modulates endoplasmic reticulum (ER) content and distribution within axons. *PLoS One, 6*(2), e17087. doi: 10.1371/journal.pone.0017087

Reddy, P. H., Reddy, T. P., Manczak, M., Calkins, M. J., Shirendeb, U., & Mao, P. (2011). Dynamin-related protein 1 and mitochondrial fragmentation in neurodegenerative diseases. *Brain Res Rev, 67*(1-2), 103-118. doi: 10.1016/j.brainresrev.2010.11.004

Rizzuto, R., Marchi, S., Bonora, M., Aguiari, P., Bononi, A., De Stefani, D., . . . Pinton, P. (2009). Ca(2+) transfer from the ER to mitochondria: when, how and why. *Biochim Biophys Acta, 1787*(11), 1342-1351. doi: 10.1016/j.bbabio.2009.03.015

Romano, A., Tessa, A., Barca, A., Fattori, F., de Leva, M. F., Terracciano, A., . . . Verri, T. (2013). Comparative analysis and functional mapping of SACS mutations reveal novel insights into sacsin repeated architecture. *Human mutation, 34*(3), 525-537. doi: 10.1002/humu.22269 [doi]

Schindelin, J., Arganda-Carreras, I., Frise, E., Kaynig, V., Longair, M., Pietzsch, T., . . . Cardona, A. (2012). Fiji: an open-source platform for biological-image analysis. *Nat Methods, 9*(7), 676-682. doi: 10.1038/nmeth.2019

Shimazaki, H., Sakoe, K., Niijima, K., Nakano, I., & Takiyama, Y. (2007). An unusual case of a spasticity-lacking phenotype with a novel SACS mutation. *J Neurol Sci, 255*(1-2), 87-89. doi: 10.1016/j.jns.2007.02.002

Song, Z., Ghochani, M., McCaffery, J. M., Frey, T. G., & Chan, D. C. (2009). Mitofusins and OPA1 mediate sequential steps in mitochondrial membrane fusion. *Mol Biol Cell, 20*(15), 3525-3532. doi: 10.1091/mbc.E09-03-0252

Szabados, T., Dul, C., Majtenyi, K., Hargitai, J., Penzes, Z., & Urbanics, R. (2004). A chronic Alzheimer's model evoked by mitochondrial poison sodium azide for pharmacological investigations. *Behav Brain Res, 154*(1), 31-40. doi: 10.1016/j.bbr.2004.01.016

Takiyama, Y. (2006). Autosomal recessive spastic ataxia of Charlevoix-Saguenay. *Neuropathology : official journal of the Japanese Society of Neuropathology*, *26*(4), 368-375.

Tan, W., Pasinelli, P., & Trotti, D. (2014). Role of mitochondria in mutant SOD1 linked amyotrophic lateral sclerosis. *Biochim Biophys Acta, 1842*(8), 1295-1301. doi: 10.1016/j.bbadis.2014.02.009

Terracciano, A., Casali, C., Grieco, G. S., Orteschi, D., Di Giandomenico, S., Seminara, L., . . . Santorelli, F. M. (2009). An inherited large-scale rearrangement in SACS associated with spastic ataxia and hearing loss. *Neurogenetics, 10*(2), 151-155. doi: 10.1007/s10048-008-0159-8

Thiffault, I., Dicaire, M. J., Tetreault, M., Huang, K. N., Demers-Lamarche, J., Bernard, G., . . . Brais, B. (2013). Diversity of ARSACS mutations in French-Canadians. *The Canadian journal of neurological sciences.Le journal canadien des sciences neurologiques, 40*(1), 61-66. doi: A327392540401020 [pii]

Timmerman, V., Strickland, A. V., & Zuchner, S. (2014). Genetics of Charcot-Marie-Tooth (CMT) Disease within the Frame of the Human Genome Project Success. *Genes (Basel), 5*(1), 13-32. doi: 10.3390/genes5010013

Tradewell, M. L., Durham, H. D., Mushynski, W. E., & Gentil, B. J. (2009). Mitochondrial and axonal abnormalities precede disruption of the neurofilament network in a model of charcot-marie-tooth disease type 2E and are prevented by heat shock proteins in a mutant-specific fashion. *J Neuropathol Exp Neurol, 68*(6), 642-652. doi: 10.1097/NEN.0b013e3181a5deeb

Vehvilainen, P., Koistinaho, J., & Gundars, G. (2014). Mechanisms of mutant SOD1 induced mitochondrial toxicity in amyotrophic lateral sclerosis. *Front Cell Neurosci, 8*, 126. doi: 10.3389/fncel.2014.00126

Vermeer, S., Meijer, R. P., Pijl, B. J., Timmermans, J., Cruysberg, J. R., Bos, M. M., . . . Kremer, B. (2008). ARSACS in the Dutch population: a frequent cause of early-onset cerebellar ataxia. *Neurogenetics, 9*(3), 207-214. doi: 10.1007/s10048-008-0131-7

Verstreken, P., Ly, C. V., Venken, K. J., Koh, T. W., Zhou, Y., & Bellen, H. J. (2005). Synaptic mitochondria are critical for mobilization of reserve pool vesicles at Drosophila neuromuscular junctions. *Neuron, 47*(3), 365-378. doi: 10.1016/j.neuron.2005.06.018

Wang, W., Li, L., Lin, W. L., Dickson, D. W., Petrucelli, L., Zhang, T., & Wang, X. (2013). The ALS disease-associated mutant TDP-43 impairs mitochondrial dynamics and function in motor neurons. *Hum Mol Genet, 22*(23), 4706-4719. doi: 10.1093/hmg/ddt319

Wolozin, B. (2012). Regulated protein aggregation: stress granules and neurodegeneration. *Mol Neurodegener, 7*, 56-1326-1327-1356. doi: 10.1186/1750-1326-7-56 [doi]

Yu-Wai-Man, P., Pyle, A., Griffin, H., Santibanez-Korev, M., Horvath, R., & Chinnery, P. F. (2014). Abnormal retinal thickening is a common feature among patients with ARSACS-related phenotypes. *Br J Ophthalmol, 98*(5), 711-713. doi: 10.1136/bjophthalmol-2013-304534 [doi]

Yuan, A., Sasaki, T., Kumar, A., Peterhoff, C. M., Rao, M. V., Liem, R. K., . . . Nixon, R. A. (2012). Peripherin is a subunit of peripheral nerve neurofilaments: implications for differential vulnerability of CNS and peripheral nervous system axons. *J Neurosci, 32*(25), 8501-8508. doi: 10.1523/jneurosci.1081-12.2012

Zhai, J., Lin, H., Julien, J. P., & Schlaepfer, W. W. (2007). Disruption of neurofilament network with aggregation of light neurofilament protein: a common pathway leading to motor

neuron degeneration due to Charcot-Marie-Tooth disease-linked mutations in NFL and HSPB1. *Hum Mol Genet, 16*(24), 3103-3116. doi: 10.1093/hmg/ddm272